Geosci. Model Dev. Discuss., 6, 5489–5551, 2013
www.geosci-model-dev-discuss.net/6/5489/2013/
doi:10.5194/gmdd-6-5489-2013

Geoscientific Model Development
Discussions
Open Access

APIFLAME v1.0: high resolution fire emission model and application to the Euro-Mediterranean region

S. Turquety[1], L. Menut[2], B. Bessagnet[3], A. Anav[2,*], N. Viovy[4], F. Maignan[4], and M. Wooster[5]

[1]Université Pierre et Marie Curie-Paris 6, Laboratoire de Météorologie Dynamique, IPSL, CNRS, UMR8539, 4 Place Jussieu, 75252 Paris Cedex 05, France
[2]Laboratoire de Météorologie Dynamique, IPSL, CNRS, UMR8539, 91128 Palaiseau Cedex, France
[3]Institut national de l'environnement industriel et des risques, Parc technologique ALATA, 60550 Verneuil en Halatte, France
[4]Laboratoire des Sciences du Climat et de l'Environnement, IPSL, CEA-CNRS-UVSQ, UMR8212, Gif sur Yvette, France
[5]King's College London, Environmental Monitoring and Modelling Group, Department of Geography, KCL, Strand, London, WC2R 2LS, UK
[*]now at: University of Exeter, College of Engineering, Mathematics and Physical Sciences, Exeter EX4 4QF, UK

Received: 8 October 2013 – Accepted: 14 October 2013 – Published: 6 November 2013

Correspondence to: S. Turquety (solene.turquety@lmd.polytechnique.fr)

Published by Copernicus Publications on behalf of the European Geosciences Union.

Abstract

This paper describes a new model for the calculation of daily, high-resolution (up to 1 km) fire emissions, developed in the framework of the APIFLAME project (Analysis and Prediction of the Impact of Fires on Air quality ModEling). The methodology relies on the classical approach, multiplying the burned area by the fuel load and the emission factors specific to the vegetation burned. Emissions can be calculated on any user-specified domain, horizontal grid, and list of trace gases and aerosols, providing input information on the burned area (location, extent) and emission factors of the targeted species are available. The strength of the proposed algorithm is its high resolution and its flexibility in terms of domain and input data (including the vegetation classification). The modification of the default values and databases proposed does not require changes in the core of the model.

The code may be used for the calculation of global or regional inventories. However, it has been developed and tested more specifically for Europe and the Mediterranean area. In this region, the burning season extends from June to October in most regions, with generally small but frequent fires in Eastern Europe, Western Russia, Ukraine and Turkey, and large events in the Mediterranean area. The resulting emissions represents a significant fraction of the total yearly emissions (on average amounting to ~30 % of anthropogenic emissions for $PM_{2.5}$, ~20 % for CO). The uncertainty on the daily carbon emissions was estimated to ~ 100 % based on an ensemble analysis. Considering the large uncertainties on emission factors, the potential error on the emissions for the various pollutants is even larger. Comparisons to other widely used emission inventories shows good correlations but discrepancies of a factor of 2–4 on the amplitude of the emissions, our results being generally on the higher end.

1 Introduction

Fires are a major source of trace gases and aerosols, critically perturbing atmospheric composition (Seiler and Crutzen, 1980; Andreae and Merlet, 2001), with various impacts on the atmospheric environment (Turquety, 2013, and references therein). The relatively long lifetime of several key emitted species allows long-range transport of the fire plumes, which thus may have significant impact at regional to hemispheric scales (e.g., Langmann et al., 2009; Jaffe and Wigder, 2012) and control interannual variability for various species (e.g., Spracklen et al., 2007; Szopa et al., 2007; Jaffe et al., 2008). The dense fire plumes may in turn influence the radiative budget, and thus climate and mesoscale meteorology (Koren et al., 2004; Tosca et al., 2013), as well as cloud microphysics (Andreae et al., 2004; Grell et al., 2011). But the most direct impact of fire emissions remains the degradation of local and regional air quality. In order to understand these impacts and the associated physical and chemical processes, accurate biomass burning emissions need to be integrated into chemistry transport models (CTMs). In this publication, we present a new model for the calculation of daily high-resolution emissions of trace gases and aerosols, which was developed more specifically to meet the needs of air quality monitoring. The emission model may be used for any region of the globe but a particular emphasis is placed here on the Euro-Mediterranean region.

Unlike in some tropical or boreal regions, fires in Europe are not the dominant source of pollution in terms of total mass emitted. However, fires become an important source during the fire season, extending typically from June to October, which can reach extreme values during the main burning events (usually in the summer). According to the monitoring and yearly reports from the European Forest Fire Information System (EFFIS) operated by the Joint Research Center (JRC), the most affected countries are Spain, Italy, Portugal, Greece and France. Almost 85 % of the total burned area is located in the Mediterranean area. However, fires in Eastern Europe and Western Russia are also frequent during spring and summer (Stohl et al., 2007; Amiridis et al., 2010). Although the number of fires has decreased in the past decades due to fire suppression policies, the yearly area burnt has remained constant due to a constant number of large fire events. San-Miguel-Ayanz et al. (2013) estimate that about 2 % of “mega-fires” contribute to 80 % of the total area burnt. These events correspond to clusters of fires that burn simultaneously and propagate rapidly due to critical meteorological conditions – hot and dry conditions with strong winds (Pereira et al., 2005) – and are thus particularly difficult to control. During large wildfire events, such as the Portuguese fires in 2003, the Greek fires in 2007 or the Russian fires in 2010, contribution from fires emissions were comparable to anthropogenic activities but concentrated in time and space (Hodzic et al., 2007; Turquety et al., 2009; Hodnebrog et al., 2012; Konovalov et al., 2011; R’Honi et al., 2013). It is critical to evaluate their impact as the large fires often occur close to densely populated areas, and during hot and dry summers, in conditions already favorable to the development of photochemical pollution episodes. In the directive 2008/50/EC (EC, 2008), PM_{10} (particulate matter with diameter lower than 10 µm) exceedances of the daily and yearly limit values that have a natural origin can be substracted when assessing compliance with air quality limit values. Forest fires can fall in this category of particles or at least they can explain significant exceedances.

For air quality monitoring applications, knowledge of the emitted mass for the main pollutants has to be provided at high horizontal resolution in order to accurately simulate the plume transport pathways (correct location and spread), and high temporal resolution to capture the large variability of fire activity. Calculating the emissions requires the knowledge of the quantity and type of vegetation burned, but also of the type of fire (smoldering vs. flaming). However, except for the study of specific, fully monitored fires, these informations are often missing and need to be estimated.

The availability of satellite-based fire monitoring since the mid-1990s, of active fires and associated area burned (e.g. Giglio et al., 2006, 2010) has allowed the development of more and more realistic inventories of the resulting emissions (Hoelzemann et al., 2004; Mieville et al., 2010; van der Werf et al., 2006, 2010;

Wiedinmyer et al., 2011; Urbanski et al., 2011). Most inventories are based on the initial formulation of Seiler and Crutzen (1980), which derives emissions from the initial burned area. Recent studies have used an alternative approach, relying on the instantaneous fire radiative power (FRP), a measure of the rate of radiant energy emission from the fire, to derive directly the amount of fuel burnt (Freeborn et al., 2008). This approach is mainly used for operational monitoring purposes (Kaiser et al., 2012; Sofiev et al., 2009).

In spite of the increasing number of satellite observations of fire activity, uncertainties on biomass burning emissions remain large. They are associated with both the evaluation of the burnt area and the corresponding fire characteristics (vegetation burnt and fuel load) and emission factors (Langmann et al., 2009). Providing uncertainty assessment is particularly difficult, mostly due to the lack of references from in situ measurements. Intercomparisons exercises have shown large dispersions of burned areas estimates (Hyer and Reid, 2009; Giglio et al., 2010) or resulting emissions (Stroppiana et al., 2010). In their intercomparison, Stroppiana et al. (2010) find that European biomass burning emissions of carbon monoxide (CO) for the year 2003 range from 1.6 to 87.8 Tg depending on the methodology and area burned product used. van der Werf et al. (2010) have used a Monte Carlo approach to evaluate the impact of uncertainties in each step of the calculation on the resulting emissions. They estimate an uncertainty of $\sim 20\,\%$ on the total yearly carbon emissions. Using the same method, Urbanski et al. (2011) estimate the uncertainty of western United States emissions to $< 50\,\%$ for CO, increasing to $< 133\,\%$ for daily emissions at 10 km resolution for 50 % of the total CO emissions. Uncertainties on daily emissions are generally estimated to be of a factor of 2 (Wiedinmyer et al., 2011).

In this publication, the diurnal to interannual variability of fires in the Euro-Mediterranean region is first described based on satellite remote sensing of fire activity. We then provide a full description of a new model for the calculation of emissions at high spatial and temporal resolution, developed in the framework of the APIFLAME project (Analysis and Prediction of the Impact of Fires on Air quality ModEling). The approach chosen is based on the Seiler and Crutzen (1980) classical approach with the biomass density simulated by the ORCHIDEE global dynamic vegetation model (Krinner et al., 2005; Maignan et al., 2011). The APIFLAME emissions' model was designed to allow flexibility of the key fire characteristics. The emissions obtained for key pollutants are presented for the 2003–2012 time period. An analysis of the related uncertainty is undertaken using two complementary approaches: a comparison with other widely used inventories, and the calculation of an ensemble of results obtained when changing the input information for burned areas and fuel load. This uncertainty assessment is done for the case study of the summer 2007, which was among the worst fire seasons of the past decades in Europe.

2 Vegetation susceptible to burning

Fire behavior and the amount of trace gases and aerosols emitted by a given fire strongly depend on the burned vegetation (type and density of fuel). For specific areas and specific fires, this information may be provided by forestry services. However, for large regions, it is necessary to rely on more systematic and self-consistent landuse databases and modeling of the carbon cycle and vegetation dynamics (e.g. Sitch et al., 2003; Krinner et al., 2005; Li et al., 2012). This section briefly describes the approach used in this work.

2.1 Vegetation type databases

Several land cover databases are available. In this study, the main constraint was to use a high resolution land cover map to attribute as precisely as possible the type of vegetation burnt for Europe.

For Europe, we have chosen to use the satellite-based CORINE (coordination of information on the environment) land cover database (CLC) (EEA, 2007). It provides the land cover class at a resolution of 250 m. The 2006 database is used when available, the 2000 database otherwise (Greece for instance). The 44 original classes have been merged into 14 vegetation classes, listed in Table 1. Artificial and sparsely vegetated classes are also included but are not allowed to burn (assume false detection). For convenience, the CLC database has been regridded at 1 km × 1 km. The fraction of each vegetation type within each grid cell is then used for landuse attribution.

Outside of the region covered by this database, we use the yearly percent vegetation cover from the MODIS (Moderate Resolution Imaging Spectroradiometer) satellite instrument, the collection 5 land cover type product MCD12Q1 (referred to as MODIS MCD12 in the following) (Friedl et al., 2010). The year 2006 is used here, but the code can run with year-specific database. Among the provided vegetation types, we arbitrarily chose to use the IGPB (International Geosphere–Biosphere Program) land cover classification.

The fraction of vegetation cover, represented on a $0.1^\circ \times 0.1^\circ$ grid, is shown in Fig. 1 for both CLC and MODIS MCD12 databases. While the general patterns are consistent for all databases (dominance of forest, especially North of 50° N, croplands and grasslands in the mid-latitudes and of shrublands in the Mediterranean area), there are significant differences in the relative fractions and distributions in some regions. For example, the distribution of croplands in Spain and Ukraine are significantly different.

However, since vegetation classes are not always the same, exact comparisons can be difficult. For example, pasture in the CLC is attributed in these maps to the grassland type and natural grasslands to savanna. In the MODIS/IGBP classification, both savanna and grassland are provided. Grassland corresponds to herbaceous areas with tree and shrub cover lower than 10 %. In the savanna class, forest can be 10–30 % of the vegetation cover (forest canopy ≥ 2 m). Natural grassland in CLC correspond to areas with a least 75 % herbaceous vegetation. There is thus uncertainty in the exact correspondence between the different classifications.

In addition to these L3 observations, the USGS (US Geological Survey) land use classification at 1km × 1 km can also be used in the emissions' model. The sensitivity to using either one of these distributions in the calculation of the emissions is tested in Sect. 7.2.

The MODIS vegetation continuous field (VCF) data at 500 m resolution (MOD44B L3 dataset) (Hansen et al., 2003), providing the fraction of pixel covered by vegetation, are also used for area burned processing.

2.2 Biomass density

For the evaluation of the biomass density in an area affected by fires, simulations by the ORCHIDEE global dynamic vegetation model (Krinner et al., 2005; Maignan et al., 2011) have been used. ORCHIDEE allows the simulation of the interactions between surface and atmosphere, the continental carbon cycle and the long-term evolution of vegetation. It consists of three modules: the SECHIBA model describes the hydrology; the STOMATE model simulates the daily phenology and continental carbon cycle, and the LPJ model for the long-term vegetation dynamics. Two ORCHIDEE simulations are used in this study: a global simulation at 70 km and a regional simulation at 30 km for the Euro-Mediterranean area (Anav et al., 2010).

The global simulation, detailed in Maignan et al. (2011), is provided to allow full flexibility of the methodology in terms of area of interest, although the inventory is primarily developed for Europe. It is based on the ORCHIDEE 1.8.2 release, with an improved phenological model for crops. The simulation is forced by ECMWF ERA-Interim meteorological fields (Berrisford et al., 2009), over the 1989–2008 period, starting from an equilibrium state for all carbon reservoirs. The soil map, giving fractions of sand, silt and clay, is derived from Zobler (1986). A global annual mean is considered for the CO_2 atmospheric concentration.

The regional simulation was based on a $0.25^\circ \times 0.25^\circ$ climate forcing by the REMO regional climate model (Jacob and Podzun, 1997), provided in the frame of the CEXTREM European project. The simulation is started with a spinup to a neutral net CO_2 exchange in 1901 and then run using changing climate and CO_2 but with fixed land cover. The soil map is derived from European 1 : 1 000 000 soil database (Panagos, 2006).

For both global and regional simulations, the PFT distribution over Europe is derived from the Corine Land Cover (CLC) map. A global annual mean is considered for the CO_2 atmospheric concentration.

According to the vegetation type associated with a specific fire (Sect. 2.1), a corresponding PFT is attributed. Therefore, a matrix of correspondence between vegetation class and PFT, described in Table 1, is used. For example, if a fire is found to be burning in “Mixed cropland and forest”, the biomass density will be evaluated as the sum of the biomass densities in PFT “Agriculture” and “Forest”. Since agricultural fires are often less intense and may not burn the full area, the contribution from this PFT is divided by two.

All forest types are merged together in order to avoid uncertainties in the forest type classification. But attribution to either tropical, temperate and boreal forest is used for the emission factors attribution (Sect. 5.2).

Among the carbon pools included in the model, we assume that four classes are subject to burning: litter, wood, leaves, and roots. The wood, leaves and roots carbon pools are the largest contributions for forest PFT (Hoelzemann et al., 2004; Li et al., 2012). Wood contributes to a very small fraction for both grasslands and croplands. The seasonal cycle varies depending on the pool: maximum carbon content is reached in Spring for wood, Summer for leaves and roots and Winter for litter. A slight increase during the past decade is associated with the response to increasing CO_2, accounted for in the simulations. Ground layer burning other than roots is not considered in the present version of the inventory, it will be included in subsequent version to allow accurate application of the algorithm to boreal regions for example, where ground layer burning is critical (e.g. Soja et al., 2004).

3 Remote sensing observations of fire activity

Reports of fire locations, size and durations are often available from forestry agencies and fire fighter's reports. However, for regional applications, only satellite remote sensing can provide a complete and self-consistent picture of fire activity, with precise location and temporal variability. The burned areas derived directly from satellite are now showing good performance (Giglio et al., 2010), although uncertainties inherent to satellite observations remain (Hyer and Reid, 2009).

When detailed reports are available for the region analyzed, combining reports with precise location from satellite can provide more realistic quantification of areas burnt (e.g. Turquety et al., 2007). For time periods with no satellite observations available, statistical analysis of fire reports and tree-ring reconstructions have been used to analyze fire history (Mouillot and Field, 2006).

The emissions' model presented here may be used with any areas burned database, provided the date of burning, location and corresponding area is known. For the application to Europe and the Mediterranean area, we have chosen to use satellite remote-sensing observations. The fire characteristics will be described in terms of both active fires and burned areas. Both products are briefly described in this section.

3.1 Active fires

There are several satellite sensors allowing the monitoring of active fires based on thermal anomaly measurements ("hotspots") (Roy et al., 2013). Here, we have focused on two complementary observations.

The active fire products from the Moderate Resolution Imaging Spectroradiometer (MODIS), carried on board the Terra satellite platform since 2000 and Aqua since 2003, has been used. More specifically, we used the MOD14 product (Giglio et al., 2006) at 1km × 1 km resolution, which provided both the location of the thermal anomalies, and the association fire radiative power (FRP) observations. The FRP provides direct information on the fire heat energy, and so of its intensity, that has been linked to the fire combustion rate (Wooster et al., 2005; Freeborn et al., 2008).

The SEVIRI/MSG geostationary observations also allow a monitoring of thermal anomalies and FRP (Wooster et al., 2005; Roberts et al., 2005), as well as their evolution during the course of a day with measurements every 15 min. However, the pixel size of 3 km is coarser than for MODIS, resulting in a higher detection limit (small fires may be missed). Both detections are thus complementary and are here used in conjunction.

These thermal radiation measurements are only available under cloud free conditions, which may induce uncertainties in the temporal variations of fires. However, they are the only measurements available in near-real time and are thus used in many operational monitoring systems or emission inventories (e.g. Sofiev et al., 2009; Wiedinmyer et al., 2011; Kaiser et al., 2012).

3.2 Burned area

Several recent satellite products provide estimates of the burned areas based on burned scars. In particular, two products based on MODIS satellite observations are increasingly used in the community: the MODIS MCD45 product (Roy et al., 2008), and the MODIS MCD64 product (Giglio et al., 2010). According to the intercomparison in Giglio et al. (2010), the variability of area burned is consistent in both products, but MCD45 tends to be higher. Both datasets provide the date of burning within 500 m × 500 m grid cells, and an associated level of confidence. An inherent uncertainty is associated with the satellite pixel size: within the 500 m × 500 m areas, heterogeneities can be large, implying uncertainty on the actual area burnt, and on the associated vegetation.

Following the approach of Wiedinmyer et al. (2011), area burned maps are derived by combining the burnt pixel detection with the MODIS VCF product (Hansen et al., 2003) in order to determine the fraction of vegetation in each cell. Only that fraction is assumed to have burnt (bare fraction is not burnt). In this paper, the different burned area datasets are referred to as MCD45 and MCD64, but correspond to the scaled area burned values. Both MCD45 and MCD64 products have been used in the emission model for uncertainty analysis (Sect. 3). In Sect. 4, the variability of the area burned in Europe is analyzed based on the scaled MCD64 data.

3.3 False detections

Even using the higher confidence observations in the available datasets, some false detections remain, especially for the active fires. These often correspond to power plants, gas flares or other industrial activities. To avoid computing emissions at these locations, successive tests are undertaken. False detection is assumed if:

- the fire is detected in an urban or a sparsely vegetated class;
- the urbanized fraction in the corresponding landcover (1 km resolution) is larger than 20 %;
- the fire is location within 1 km of an industrial facility using the European Pollutant Release and Transfer Register (e-PRTR http://prtr.ec.europa.eu/) database;
- the statistical analysis of MODIS active fires (at 10 km resolution) for the past 10 yr shows unrealistically high frequency of fires throughout the year (burning $\geq$ 40 % of the days).

This may result in a slight underestimate in the case of fires close to inhabited regions.

4 Overview of fire activity in the Euro-Mediterranean region

Variability of the fire activity is the main driver for variability in fire emissions. Therefore, spatial and temporal variations are first analyzed, using the observations of area burned (MODIS MCD64 product) and active fires (MODIS MOD14 product) for the 2003–2012 time period, averaged over a 0.1° × 0.1° grid.

4.1 Seasonal and interannual variability

Figure 2 shows the averaged total yearly area burnt (for each grid cell: the total area burnt during the period is divided by the number of years with fires detected), as well as the probability of detecting at least one fire during the year within each grid cell. The main regions affected by vegetation fires are Southern countries (Iberian Peninsula and the Mediterranean area) and the Eastern countries (Eastern Europe, Russia, Ukraine). Large burned areas are mainly observed in the Southern countries, but are less frequent than the small fires occurring in the Eastern part of the region.

The total yearly burned areas by country have been compared to the European Fire Database from the EFFIS/JRC which reports the forest fire data provided each year by individual countries (Schmuck et al., 2013). Table 2 summarizes results for countries with the most significant burning. For the Southern countries, Portugal, Spain, France, Italy, the republic of Moldova, Greece, the agreement between the reports and the MODIS MCD64 observations is good, with correlations larger than 0.92. We note a tendency to underestimate burned areas compared to the reported totals, by 20–30 % for most countries, except Greece. For countries in Eastern Europe and Turkey, the correlation is low and the reported totals are a lot lower than the observed values. This difference may be explained by the fact that the EFFIS reports only include burned areas in natural vegetation, while a lot of burning in Eastern Europe is associated to agricultural practice, as discussed in the following section. Further validation would be required to better assess the quality of the burned area data in Europe, especially in Eastern countries.

Total monthly burned areas for the 2003–2012 time period and the main burning regions are presented in Fig. 3. In all regions, the maximum fire activity is reached during the Summer months, but the fire season usually extends from June to September in the Southern countries; until October in the Eastern countries and

Portugal. Significant burning also occurs in Spring (March–April) in the Eastern part of the domain (mostly agricultural fires). Interannual variability is also lower in these regions, with fires detected almost every year during the past decade. Southern countries, where fires are less frequent, are characterized by a strong interannual variability. Several intense fire years are clearly noticeable: 2007 in the central and Eastern Mediterranean area, 2003 and 2005 in Portugal, 2012 in Spain, Italy and Eastern Europe.

The observed maximum FRP follows similar pattern, with maximum values in August. FRP remains large during winter, although the number of fires detected decreases significantly. These detections may correspond to isolated fires or false detections that are not correctly filtered out.

The fire duration has been estimated as the number of consecutive days with a fire detected within a given pixel. The average fire duration is mapped in Fig. 2 for the 2003–2012 time period. In order to avoid false variability due to detection (the presence of a cloud for instance), a 1 day gap is allowed. Although this does not provide a precise quantification of individual fire duration (several fires can occur within the considered grid cell, and large fires may spread through grid cells), this simple method gives a general overview of the durations of the events in the different regions. Figure 2 shows the spatial distribution on average for the years 2003–2012. The smaller fires in the Eastern regions last generally for about 2 days, while large fires in the Southern countries can be detected during 4–10 days. These large fires, burning for long time periods, correspond to clusters of small fires resulting in mega fire events, as analyzed by San-Miguel-Ayanz et al. (2013).

4.2 Vegetation type burned

Figure 4 shows the relative contribution of each vegetation type in terms of area burned detection, using the CLC database when available and MODIS MCD12 elsewhere (in this case North Africa, Ukraine and Russia).

During the summer months (July–August), about 48.5 % of the fires are detected in croplands, 21.1 % in forests, 20 % in grasslands, 9 % in shrubland and 1.4 % in natural grassland. Fires in cropland are dominant in the eastern part of the domain, more specifically Eastern Europe, Ukraine, Western Russia, and Turkey, but also in Southern Italy. Appart from Italy, forest and grassland fires are dominant in the Mediterranean countries. Forest fires contribute to 39 % of the fires in Portugal, 30 % in Spain, 25 % in Southern France, Corsica and Sardinia, and to 22 % in Greece. Mediterranean shrubland only contributes a small fraction according to the CLC database, 10–13 % on average in the Mediterranean area, while grassland contributes to about 35–50 %.

Fires in Spring mainly occur in croplands in Eastern Europe and Ukraine. The fraction of croplands also tends to increase later in the season (September–November).

These general features remain consistent if MODIS or USGS land covers are used. The main difference is that MODIS or USGS attribute larger fractions of area burned in shrubland in the Mediterranean countries, that corresponds to grassland in the CLC classes. USGS also tends to attribute more fires in croplands.

As already mentioned, the difficulty to precisely attribute the burned vegetation on a regional scale is one of the main uncertainties of the methodology. The uncertainty associated with the choice of landuse will be further discussed in Sect. 7.

4.3 Diurnal variability

Geostationary observations of the fire radiative power from SEVIRI are used to estimate the diurnal cycle. The hourly variability of the number of detected fires, and the corresponding average variability of FRP within the main burning regions are shown in Fig. 5.

For all regions, the diurnal cycle of the number of fires detected is very pronounced, with a peak in the afternoon, between 14:00 and 16:00 local time (LT). In Italy and in the Eastern part of the domain, the number of fires is high throughout the day, with a secondary maximum in the morning (08:00–10:00 LT). The large fraction of fires attributed to cropland in these regions may explain the differences. The number of fires detected at night remain significant, except for Eastern Europe.

In terms of FRP, the diurnal cycles are less contrasted and the peak values are on average observed earlier in the afternoon (1–4 p.m.). The profiles are more consistent between regions, except for Southern Italy.

Mu et al. (2011) analyzed diurnal variations (03:00 LT) of fires above North America using the GOES geostationary observations (WF-ABBA). They find a clear peak in the afternoon (12:00–16:00 LT) for all regions and all types of vegetation, going down to almost zero at night in croplands in North America and for all vegetations in Central and South America. Our results suggest that these profiles can not be applied to Europe. Roberts et al. (2009) analyzed the diurnal cycle of fires in Africa using the SEVIRI observations and showed a peak at around 14:00 LT and low fire activity between midnight and 07:00 LT. These results were consistent in terms of number of detections and FRP value, and for all vegetation types. They note however that some strong variability can be observed due to cloud cover contamination.

Detection is also more difficult for smaller, smoldering fires, that can still emit large amounts of trace gases and aerosols. A smaller amount of fires detected during the night can thus suggest that flaming fires are lower, but smoldering can remain. For wildfires remaining active several days, emissions should not become zero at night.

For this reason, and because FRP is directly linked to the fuel consumption, we have chosen to estimate the diurnal cycle based on the FRP rather than the number of fires. The FRP hourly variation's profiles are normalized and used in the emission model to estimate the diurnal cycle of the emissions.

5 High resolution emission model

This section describes the first version (v1.0) of the APIFLAME emission model. The approach used follows the formulation of Seiler and Crutzen (1980). For each emitted species *i* considered (trace gas or aerosol), the emission associated with a detected fire E_i (g) is estimated by multiplying the total area burned A (m^2) by the fraction in each vegetation type v, f_v, the fuel load, i.e. the quantity of biomass susceptible to burning or fuel consumption factor F_v (kg dry matter (DM) m^{-2}), which also depends on vegetation, and the specific emission factor for the considered species and vegetation type $\epsilon_{v,i}$ (g (kg DM)$^{-1}$), as summarized in the following equation:

$$E_i = A \sum_{v=1}^{\text{veg\_types}} f_v F_v \epsilon_{v,i} \tag{1}$$

Any chemical species may be included in the inventory if the corresponding emission factor for each vegetation class, $\epsilon_{v,i}$, is known. Eq. (1) is applied at fire resolution: for each fire detection, each parameter of the calculation are estimated to calculate the corresponding emissions for a list of species. The emissions are then binned into a specified grid, with resolution ranging from a few kilometers to several hundreds kilometers, depending on applications. For a given fire location and associated area burned, the steps necessary for the computation of Eq. (1) are described in the following subsections. A general scheme of the emission model is provided in Fig. 6.

5.1 Fuel load

The fuel load is calculated by multiplying the biomass density (B_p in kg C m^{-2}) of each considered carbon pool p in the region of the fire by the fraction of vegetation that is expected to actually burn (burning fraction β) such that

$$F_v = \sum_{p=1}^{\text{carbon\_pools}} B_{p,v} \beta_p \tag{2}$$

The fuel load is converted from kg C m^{-2} to kg DM m^{-2} assuming a 48 % carbon content in DM (following van der Werf et al., 2010).

The biomass density is estimated using the ORCHIDEE model, as described in Sect. 2.2. Although global datasets of soil (Nachtergaele et al., 2012) and vegetation carbon content (Gibbs, 2006) exist at fine spatial resolution, here we used the ORCHIDEE model to estimate the biomass density because these datasets do not discriminate the fraction of each pool (p) contributing to the total carbon content.

The combustion completeness (or burning efficiency) corresponds to the ratio of fuel load to total available biomass. It is difficult to estimate since it is influenced by vegetation characteristics such as age, phenology, and moisture content. But it also depends on fire behavior, such as fire line intensity, fire rate of spread, and flame residence time. This will in turn affect the relative contribution of flaming and smoldering combustion, with a higher burning efficiency indicating more flaming (Yokelson et al., 1996). The burning efficiencies are often estimated from fuel consumption measurements in prescribed or experimental fires (Rosa et al., 2011). In general, fine and dry fuels burn more completely than coarse and wet fuels (van der Werf et al., 2006).

The fraction of biomass available for burning is first estimated using values recommended by Hoelzemann et al. (2004), and indicated in Table 3 for the ORCHIDEE PFTs. Minimum and maximum values show a large range of variations. A simplified parameterization (linear interpolation) based on moisture stress is used to determine whether combustion is closer to the lower or upper limit: the minimum scenario is used for wet regions/seasons, while the maximum scenario is used for the dry ones. Vegetation moisture stress from the ORCHIDEE simulations is used. It is calculated from relative soil moisture by convolution of this relative soil moisture to an exponential root density decrease. The exponent coefficient depends of the PFT. For instance grass an crops are mainly sensitive to the first 50 cm of the soil whereas trees are sensitive to up to 2 m. The global simulation generally shows slightly drier conditions than the regional one, more specifically in summer. Hence, while carbon load is lower, the fraction available for burning will be higher.

A burning efficiency is then applied to the available biomass, again following Hoelzemann et al. (2004). The averaged regional values of fuel loads for each scenario are shown in Table 4 for the example of the summer 2007. For each type of vegetation, only grid cells where contributing PFTs correspond to more than 75 % of the vegetation cover are considered. The variability among scenarios is largest for the forest PFTs. Average fuel load based on the regional and the global simulations is provided in Table 5. The global simulation results in fuel loads lower by almost 50 % for forest, by about 10 % for agriculture and larger by about 26 % for grassland. Note that fuel loads are scaled by the fraction of grid cell occupied by the specific PFT (total carbon being a weighted average of the carbon density within each PFT). Due to inhomogeneosities within the grid cells, this naturally results in lower values than if only one PFT is assumed. The lower horizontal resolution of the global simulation may thus explain part of the differences in the average fuel loads provided here.

Hoelzemann et al. (2004) report values of available biomass of 0.8 and 1.4 $\mathrm{kg\,m^{-2}}$ for savanna in Western and Eastern Europe, respectively, and of 7.5 and 11.8 $\mathrm{kg\,m^{-2}}$ for forests. The values used here are thus on the lower end for forests, but in good agreement for grasslands. The uncertainty related to this parameter is explored through the calculation of the emissions for the four scenarios: tabulated minimum, average or maximum values as well as the variation according to moisture stress (cf. Sect. 7).

5.2 Emission factors

The species and corresponding emission factors used are listed in Table 6. The values from the recent review of Akagi et al. (2011) are used for most species, complemented with the Andreae and Merlet (2001) database for missing values. Emission factors are provided in terms of g species per kg DM burned ($\mathrm{g\,kg^{-1}}$) for all relevant species observed in burning plumes (from field or laboratory measurements) and for different standard vegetation types (tropical forest, temperate and extratropical forest, boreal forest, crop residue, pasture maintenance, savanna). Once the fuel burned is estimated

(DM burned), emissions for a large series of trace gases and aerosols can be calculated.

The type corresponding to a specific fire is attributed using the vegetation type provided by the landuse classification (CLC, MODIS or USGS). Correspondence between the vegetation types is indicated in Table 1 for the CLC database (used by default over Europe). For example, if a fire is detected in a "mixed cropland and forest" vegetation, the emission factor is estimated to be the average of the emission factors for crop residue and forest. If emission factors for temperate or boreal forests are not provided, values of extratropical forests are used (reported as "temperate" in the table above). If no emission factor is available for chaparral, then we use values for shrubland, which correspond to the average of savanna and temperate forest.

The emissions factors reported for chaparral in Akagi et al. (2011) are used for Mediterranean shrubland (sclerophyllous in the CLC classes, shrublands at latitudes between 30 and 35° N for other landuse databases). Values are significantly lower than for other vegetation types for compounds favored by the smoldering phase, like CO. Measurements in prescribed burning of shrubland vegetation in Portugal confirm this behavior, but report even lower values ($\sim 35\,\mathrm{g\,kg^{-1}}$ for CO) (Alves et al., 2010). Alves et al. (2011) report emission factors for typical wildfires in Portugal, which occured during the summer 2009 and mainly affected forests. These values are, on the contrary, significantly larger than those used in this study. For example, CO emission factors of $231 \pm 117\,\mathrm{g\,kg^{-1}}$ were measured, 2.6 times larger than those used here for extratropical forest. For OC, the values measured are on average $15.8\,\mathrm{g\,kg^{-1}}$, 70 % larger than those used here. There is a clear need for more observations in order to reduce the large uncertainties on emission factors.

Emissions of inventory species may then be converted to emissions of model species depending on the chemical mechanism used in the chemistry-transport model using an aggregation matrix. This matrix allows adaptability to new chemical schemes. The emission factors list and the aggregation matrix need to be modified accordingly, but no modification of the core of the emission model is required.

5.3 Diurnal cycle

Once the daily emissions are calculated using the daily burned area, the emissions may be redistributed throughout the day using a prescribed diurnal cycle.

Studies over North America have used the variability in the number of active fires detected during the day by the geostationary GOES instrument (Mu et al., 2011). For Europe, it can be estimated based on the observations by the MSG/SEVIRI instrument. As discussed in Sect. 4.3, the associated diurnal variations are very dependent on the region and the fire event considered. Although fire activity seems to decrease during the night, it is not true for all regions. The analysis of the impact of the higher temporal variability in emissions on fire plumes' transport conducted by (Mu et al., 2011) has shown that the daily variability is more critical than the hourly variability.

For these reasons, the current version of the algorithm does not provide precise processing of diurnal variability but allows the use of an average diurnal profile, adjusted for the Euro-Mediterranean region using the MSG/SEVIRI observations (cf. Sect. 4.3).

5.4 Comparing methodology to other inventories

The results obtained are compared to several widely used inventories: GFED-v3 (van der Werf et al., 2010), FINN-v1 (Wiedinmyer et al., 2011) and GFAS-v1 (Kaiser et al., 2012). These inventories are all global, daily to 3 hourly, and based on the MODIS observations of fire activity. Their main characteristics are summarized in Table 7.

GFEDv3 uses area burned data, combined to active fires for the high temporal variability (Mu et al., 2011). FINN and GFAS were designed to provided emissions on a near-real time basis. They are therefore using the active fire detection from MODIS.

GFED and FINN both use a bottom up approach, calculating emissions using Eq. (1). For FINN, the fuel load is based on the tabulated values provided by Hoelzemann et al. (2004). For GFED, modeling of the carbon cycle (the CASA-GFED model) is used, which accounts for the real fire impact. In this study, offline simulations of the ORCHIDEE model are used, without interaction with the detected fires.

GFAS uses a top-down approach, estimating carbon emissions from the fire intensity (FRP measurements). The emission factors are from the (Andreae and Merlet, 2001) database for GFED and GFAS, and from the (Akagi et al., 2011) database for FINN. In the following, the area burned estimates are compared to the GFED and FINN emissions, and emissions for the main compounds are compared to GFED, FINN and GFAS.

6 Regional fire emissions

The variability of fire emissions is mainly due to the variability of fire activity itself, discussed for Europe and the Mediterranean area in Sect. 4. In this section, the monthly CO emissions are presented and compared to the GFED and GFAS inventories. The contribution of fires to the regional pollution budget in terms of average over the past 10 yr is then discussed. Results are presented for the default configuration of the emissions' model, which uses the MODIS MCD64 area burned, the CLC vegetation database, the regional ORCHIDEE simulation with burning fraction varying depending on moisture stress. Sensitivity to the chosen configuration is discussed in Sect. 7.2.

6.1 Comparison of monthly emissions of CO

Monthly area burned described in Sect. 4 have first been compared to the GFEDv3 area burned for the 2003–2010 time period. Since the same initial area burned product from MODIS have been used (Giglio et al., 2010), these comparisons show very good correlations (> 0.98) and relative differences of 14 % on average (lower in GFEDv3).

In Southern Italy and Turkey, the correlation reaches 0.89 but the GFED monthly area burned is on average 52 % and 40 % higher, respectively. Low bias in Southern Italy is mainly due to a temporal shift, while area burned in Turkey is lower during the full fire seasons, especially before 2008. These differences may be attributed to differences in the processing of the MCD64 area burned product, more specifically the fraction of vegetated cover used to scale the 500 m × 500 m pixels. The combined use of area burned and active fires in GFEDv3 also affects temporal variability.

The resulting monthly CO emissions are shown in Fig. 7 for the calculation based on the CLC and the MODIS MCD12 vegetation types, as well as for the GFEDv3 and GFASv1 inventories. The temporal variations are consistent, in particular between this work and GFEDv3 due to the good correlations in area burned products. Correlations with GFASv1 is generally slightly lower (0.86) due to the different variability of area burned and FRP, discussed in the Sect. 4. The different approaches used in the calculation of emissions result in larger discrepancies in the emitted mass.

In the Euro-Mediterranean region, the emissions calculated in this work based on the CLC database are on averaged 2.5 times larger than GFEDv3, and 60 % larger than GFASv1. When MODIS MCD12 vegetation is used, the emissions are 3 times larger than GFEDv3 and 100 % larger than GFASv1. If only summer-time emissions are compared (largest values), the emissions based on either one of the vegetation databases are 2.5 larger than both GFEDv3 and GFASv1. This indicates that lower values are generally significantly higher in GFASv1 than in the other estimates. Again, this is due to relatively large FRP values observed throughout the year in the Euro-Mediterranean region (Fig. 3). Summer emissions are also significantly larger in GFASv1 above North Africa (70 % larger than our estimate, which is itself 4.4 times larger than GFEDv1), where very intense burning occurs in terms of FRP.

Largest differences are obtained in the Eastern regions (Eastern Europe, Ukraine, Western Russia and Turkey), especially when the MODIS vegetation classification is used, where the APIFLAME emissions are significantly higher. This is not due to the area burned since a good agreement is found in all regions with GFEDv3, and even lower than GFEDv3 in Turkey. This may be explained by discrepancies in the fuel load estimates in these regions.

A more detailed comparison of the daily emissions is presented in Sect. 7 for the case of the summer 2007, marked by particularly large fires.

6.2 Contributions to the regional emissions for the main pollutants

The partitioning in the different vegetation classes of the area burned and the associated emissions for the example of CO and NO_X, on average over the 2003–2012 time period, is indicated in Table 8. Values are given for the inventory based on the CLC vegetation types, but similar results are obtained using MODIS MCD12.

The general conclusions from the analysis undertaken in Sect. 4.2 based on areas burned are still relevant in terms of emissions. The main contributing fires are located in croplands, then shrubland, forests and savanna (natural grassland). However, the contribution from different vegetation types for a given species also strongly depends on the emission factor. For NO_X, for example, fires in shrubland are contributing almost as much as fires in croplands.

Table 9 summarizes the mean annual emissions for some of the main pollutants emitted during the fires (merging all VOCs) for the Euro-Mediterranean region (latitudes between 36 and 48° N), divided into 3 subdomains: West from 10° W to 5° E, Central from 5 to 20° E, and East from 20 to 35° E. Again, it highlights the large discrepancies between inventories in terms of total emissions. For CO, our estimates are 3.7 times larger than the GFED inventory on average over the 2003–2010 time period. For NMVOCs and TPM (total particular matter), the results depend on the number of species included so the results may not be consistent.

Table 10 provides a summary of the total annual regional emissions by country from both fires and anthropogenic activities (average for 2003–2011). This table only reports values for the countries most affected by fires and for which anthropogenic emissions from the EMEP inventory (Vestreng et al., 2007) are available. For these 14 countries, total fire emissions represent 28 % of the total anthropogenic emissions for $PM_{2.5}$ (diameter $< 2.5\,\mu m$), 21 % for CO, 14 % for NMVOCs, 7 % for coarse PM (diameter $> 2.5\,\mu m$), 3 % for NH_3, 2 % for NO_X and 0.3 % for SO_2. Hence, fires represent a significant pollution source for most regulated pollutants, all the more critical as it is concentrated in short time period. Indeed, fire events generally last less than ~ 10 days during fire seasons of only a few months (June–September), while anthropogenic emissions are almost constant throughout the year. On average over the past 10 yr, the most affected countries are Portugal, the countries of the Balkan Peninsula (Albania, Bosnia-Herzegovina, the republic of Macedonia, Greece), Moldova, Ukraine and Spain, which all have fire emissions representing more than ~ 30 % of the anthropogenic emissions for CO and $PM_{2.5}$ (up to 136 and 156 % for Portugal).

7 Uncertainty assessment on the case study of the summer 2007

The analysis of the uncertainty on the daily emissions is undertaken on the case of the summer 2007, which was affected by particularly strong fires in Central and Eastern Europe. Fires were most severe in Greece, with a total of 3138 km^2 burned according to the EFFIS Forest Fires in Europe 2007 report (2008), and extreme pollution transported across the Mediterranean basin (Turquety et al., 2009). A total of 3290 km^2 burned is estimated during the summer, in good agreement with the reported values by EFFIS (although 5 % higher). There where also large fires in North Africa, Southern Italy, the Balkans and Eastern Europe. The analysis of the summer 2007 case study will focus on these 6 subregions.

For the analysis of the general variability presented in Sect. 4, three additional subregions to the West of the domain will be added: Portugal, Spain, Southern France, Corsica and Sardinia.

7.1 Comparison of daily emissions to other inventories

The daily burned area comparison to FINNv1 and GFEDv3 (cf. Sect. 5.4 for their respective characteristics) is shown in Fig. 8 for the main burning subregions.

All three estimates are in good general agreement, showing the main events at the same time with the same order of magnitude. The correlation between the different estimates is ∼ 0.9. The total daily burned area over the Euro-Mediterranean region is on average 10 % lower than the FINN estimate, and 14 % lower than the GFED estimate. But regional differences can reach very large values if emissions are temporally shifted, like in Greece where the large event in August lasts one day longer in our estimate based on the MCD64 product.

Although GFEDv3 uses the same burned area product as the one used in this work for the monthly total, the daily variability is derived from the active fires product. Some events therefore do not have the exact same timing. The largest discrepancies are obtained over the eastern regions: Ukraine, Western Russia and Turkey, where GFEDv3 is significantly larger. This may be due to the weighting of the pixel size by the vegetated fraction used here.

The corresponding CO emissions, shown in Fig. 8, show significantly larger differences (daily regional emissions 2.5 times larger than GFED and GFAS on average, 70 % larger than FINN). A good agreement is obtained with the peak GFAS values for the strong Greek fires. One of the reasons may be the use of different vegetation attributions and thus emission factors. However, similar differences are obtained when comparing carbon emissions (i.e. fuel consumption) with GFEDv3 (daily regional values on average 5 times larger for this work) (Fig. 10). If the global ORCHIDEE simulation is used instead of the regional one, results are only slightly lower. However, using a different vegetation database significantly decreases carbon emissions. The critical parameter is thus the methodology used for the fuel load estimation in the different inventories.

In their analysis of the impact of fires on air quality, Hodnebrog et al. (2012) included the FINNv1 and GFEDv2 inventories in chemistry-transport models and conducted comparisons to satellite observations, more specifically for the Greek fires' plume. They have shown that CO emissions are significantly underestimated in both inventories, resulting in concentrations up to one order of magnitude too low. Although more in

Title Page
Abstract | Introduction
Conclusions | References
Tables | Figures
◀| |▶
◀ ▶
Back | Close
Full Screen / Esc
Printer-friendly Version
Interactive Discussion

depth evaluation against observations is required, the larger emissions in this new regional methodology appear to be in better agreement with the observations.

7.2 Ensemble approach

Different databases may be use to estimate the key parameters of Eq. (1) controlling the emissions. Inter-comparing these options shows that significant uncertainty is associated with each of these parameters. However, quantifying the individual uncertainties does not provide a reliable estimate of the resulting uncertainty on emissions. For example, for a given burned area in a given region, if the location varies by a few kilometers between fire observation sources, then a different vegetation burnt may be attributed, as well as a different fuel load, resulting in different emissions.

In this study, we have chosen to calculate an ensemble of emissions for the case of the Summer of 2007, using different options for each of the parameters of Eq. (1). Since fuel load has been identified as one of the main sources of discrepancies between various emission models, the analysis is focused on the carbon emissions, before any application of emission factors. 48 calculations were performed, changing one parameter at a time, as shown in Fig. 9. The dark shaded boxes highlight the reference setup of the emissions model: MCD64 area burned product, the CLC vegetation type and the regional ORCHIDEE simulation with the fraction available for burning depending on moisture stress (VAR).

Although these options are not always fully independent (hence minimizing uncertainties), they allow a first evaluation of the uncertainties of the model calculations and of its sensitivity to various options.

The results in terms of daily carbon emissions (or fuel consumption) within the main burning subregions are shown in Fig. 10. In Fig. 10, the profiles for this reference configuration but changing the vegetation type are highlighted, as well as the GFED carbon emissions for comparison.

The range of possible daily emissions appears to be extremely large. The total emitted carbon during July–August in the Euro-Mediterranean region varies between

12 and 63 Tg, with an ensemble average at 30 Tg. The reference inventory gives a total of 42 Tg with the CLC vegetation database, and twice lower with the MODIS vegetation database. GFED indicates a total of 10 Tg emitted. Smallest values of the ensemble are usually obtained when the global ORCHIDEE simulation is used for biomass density with the MODIS vegetation database. Note that the ORCHIDEE simulations were performed with the CLC land cover, so that better consistency is expected and may explain some of these differences.

The standard deviation of the ensemble members reaches 53 % on average for the daily emissions within the region, and varies between 50 and 84 % for the subregions considered here. In most regions, the reference inventory, using CLC, results in the highest values, while calculations based on the MODIS or USGS land covers are closer to the ensemble average and the GFED estimates. Some large peaks in the ensemble calculations are absent from the reference calculations. These are associated with large areas burned in the MCD45 area burned product that are not in the MCD64 product. A strong variability is thus related to the choice of area burned or vegetation types.

For a more precise quantification of the uncertainties, the standard deviation of the ensemble members for calculations on a 25 km resolution grid is analyzed grid cell by grid cell. The cumulative frequency distribution is presented in Fig. 11. The standard deviations associated with sub-ensembles, with only one varying parameter at a time, are also shown. The full ensemble has a standard deviation of 93 % on average, relative to the ensemble mean. It is larger than 100 % for ~ 50 % of the cases. The sub-ensemble with only area burned varying gives larger dispersions, with standard deviations of 103 % on average, and larger than ~ 140 % for ~ 50 % of the cases. The dispersion of this sub-ensemble is on larger than that of the full ensemble, indicating error compensations. The second largest dispersion comes from the vegetation database used, with average standard deviation of 44 %. In this analysis, the lowest uncertainty is associated to the fuel load, with standard deviation of 14 % on average if either one of the ORCHIDEE simulation is used, and of only 4 % for the different scenarios of combustion completeness. This low sensitivity to the different scenarios is due to the large fraction of fires in grassland and cropland, for which the scenario does not have significant impact (cf. Sect. 5.1). This is very probably underestimated since only one model is used here for biomass density, although in different configurations. Comparison with other inventories has shown that fuel load is a critical parameter. This contribution to ensemble uncertainty should be analyzed using different carbone cycle models.

van der Werf et al. (2010) evaluate the average uncertainty on the annual carbon emissions to 20 % on average using a Monte Carlo approach with 44 and 22 % uncertainty on biomass density for grassland and forest, respectively, 50 % on combustion completeness and the uncertainty in area burned provided by Giglio et al. (2010) of ∼ 10 % in the Northern Hemisphere. This estimate does not include the impact of uncertainties on the landuse assumed to have burnt. These values are lower for different reasons. First, these uncertainties are estimated on annual totals, which lowers uncertainties compared to daily or monthly totals. Secondly, the uncertainties on each parameter is lower than those used in this work.

Urbanski et al. (2011) also used a Monte Carlo approach to analyze uncertainties on regional emissions in the Western US, but worked at different spatial and temporal scales. On an annual and region-wide scale, they estimate that their uncertainty on fuel consumption ranges from 19 to 47 %, and that that on CO emissions ranges from 28 to 51 %. They show that uncertainty significantly increases at lower temporal and spatial scales. At daily and kilometric resolutions, they find uncertainties larger than 133 % for more than 50 % of the CO emissions. At these scales, they find that uncertainty is mainly driven by uncertainties in the burned area. These values are slightly larger but consistent with the results from the ensemble. None of the previous studies addressed the impact of vegetation attribution in the final uncertainty but we show that it is also an important factor.

More generally, Wiedinmyer et al. (2011) evaluate the uncertainty on daily emissions to a factor of two, which is consistent with the results of both the ensemble and the intercomparison.

8 Code structure and availability

Source code for the emission model may be obtained from the following web page: http://www.lmd.polytechnique.fr/apiflame.

The model has been written to allow full flexibility in terms of:

- species accounted for: any species may be included provided its emission factor is known;
- region analyzed: any domain may be chosen since global databases are provided;
- fire information: any list of fire location, date of burning and associated area burned may be used.

Several vegetation databases are provided (CLC, MODIS, USGS), but adding a new vegetation database only requires the addition of associated correspondence matrices between the vegetation classes, the ORCHIDEE PFT types and the vegetation types for which emission factors are provided.

All user specifications are informed in the main script. The code then calculates emission inventories in two steps (two executables):

1. Calculation of emissions for each detected fire pixel, and for inventory species; write output ascii file (required input: list of fire location, date and associated burned area);
2. Aggregation to model species and model grid; write output netcdf file (required input: output from step 1).

The simulation may be limited to the first step.

Title Page
Abstract Introduction
Conclusions References
Tables Figures
◀◀ ▶▶
◀ ▶
Back Close
Full Screen / Esc
Printer-friendly Version
Interactive Discussion

9 Conclusions

Emissions of trace gases and aerosols from wildfires represent one of the most important sources of pollutants in many regions of the globe. In this paper, a new model (APIFLAME emission model v1.0) for this additional source in chemistry-transport models is presented. It has been developed to meet the specific needs of air quality monitoring, namely the calculation of the emissions for the main atmospheric pollutants, at high horizontal and time resolution, with flexibility in terms of domain and species required. We presented a specific application to the Euro-Mediterranean area.

An analysis of fire activity in this region has been undertaken using the MODIS MCD64 area burned and MOD14 active fire products. The fire season extends from June to October in most areas, with some burning in Spring in eastern part of the region, but the most intense fires and largest areas burned occur in summer (July and August). Yearly burned areas are consistent with the forest fire reports from EFFIS/JRC (within 20–30 %) in most countries, but significantly larger in Eastern Europe and Turkey. This is probably due to the fact that agricultural fires are not reported in the forest fires database. Fires affect extended regions in Eastern Europe, Ukraine and western Russia with high frequency (every year in some regions), but with small durations and small burned areas on average, indicating many small fires. In the southern countries (Portugal and the Mediterranean areas), fires are less frequent, very localized but can last 5–10 days with large burned areas. Both types of fires (large events for several days or smaller recurrent fires) have a potentially large impact on regional pollution budgets that need to be accounted for, especially during summer. A large fraction of the fires occur in agricultural areas (about half of the detected fires), followed by forests ($\sim 21\,\%$), grasslands ($\sim 21\,\%$), and shrublands ($\sim 9\,\%$).

Fire emissions are calculated using the classical approach introduced by Seiler and Crutzen (1980) and used in many inventories. They are derived by multiplying the area burned by the amount of fuel available and the emission factors of each included species. Since fuel load and emission factors both depend on the type of vegetation burnt, a precise knowledge of this parameter is essential. The model allows the use of several databases. For Europe, the CORINE landcover database (CLC), regridded at 1 km resolution, is privileged. The MODIS MCD12Q1 database (500 m resolution) is used as default outside of the CLC domain. Landuse (input data) may be modified according for specific applications without modification of the model's core.

Depending on the vegetation burned and the location, the fuel load is derived from simulations by the ORCHIDEE model. Monthly mean outputs from global and regional simulations (over Europe) are provided, at 70 and 30 km resolution, respectively. Fuel load in terms of carbon available to burning is estimated depending on the type of vegetation burned, its location, the date of burning, as well as the fuel moisture stress.

Emission factors (g species per kg dry matter burned) then allow the calculation of emissions for a series of trace gases and aerosols. The emissions for inventory species are converted to emissions for model species adapted to specific chemical schemes included in chemistry-transport models using an aggregation matrix. These are provided as input and can be modified by users. Finally, emissions can be gridded within user specified model grid (domain and resolution).

The regional emissions for the 2003–2012 time period are discussed using the default configuration of the APIFLAME emission model: MODIS MCD64 area burned, CLC vegetation classification, regional ORCHIDEE simulation, and fuel load calculation depending on moisture stress. Fires represent a significant additional pollution source in the region, corresponding, for example, to 21 % of the annual anthropogenic emissions for CO, 28 % for $PM_{2.5}$, but mostly concentrated during the summer. On average over the past 10 yr, the countries most affected are Portugal (CO emissions from fires amounting to 156 % of anthropogenic emissions), the Balkan Peninsula, Moldova, Ukraine and Spain. Comparison of the CO emissions to emissions from several widely used inventories (GFEDv3, GFASv1, FINNv1) shows good correlations, highlighting the good consistency in spatial and temporal variability across the selected methodologies. However, the emitted mass is significantly larger, by a factor of 2.5 compared to GFEDv3 and GFASv1 on average over the whole region. Emissions are particularly large compared to other inventories in Eastern Europe, Ukraine, Western Russia and Turkey. These discrepancies are most probably attributable to uncertainties in the fuel load estimates.

A more precise analysis of the summer of 2007, characterized by strong burning in Eastern Europe and the Mediterranean area, has been undertaken. An ensemble of calculations relying on the various options allowed by the emissions model has been used in order to evaluate the uncertainty on emissions associated with each parameter of the equation.

The standard deviation of the emissions among the different members of the ensemble shows that uncertainty is close to 100 % on the daily carbon emissions, with dominant contribution from uncertainties on the area burned, and significant contribution from the vegetation database used (∼ 44 %), a source of uncertainty that had not been considered in previous uncertainty analyses based on a Monte Carlo approach (Urbanski et al., 2011; van der Werf et al., 2010). Uncertainty on the biomass density and fuel load calculation method is low but probably underestimated due to the fact that the same carbon cycle model is used (ORCHIDEE). Uncertainty on total daily emissions within the main burning subregions is estimated to ∼ 50–84 %. Carbon emissions from the GFEDv3 inventories are within the ensemble, but generally closer to the smallest values. In addition to these large uncertainties on carbon emissions, uncertainties on emission factors must be considered for trace gas and particulate matter emissions, explaining the larger differences among inventories (a factor of 2–3).

Our analysis of the active fires observations from the MSG/SEVIRI instrument suggests that fire activity is more intense during the afternoon. However, some regions show larger number and intensity of fires at night (southern Italy). It is therefore difficult to derive an averaged climatological diurnal profile representative of all fires in the region. The emission's model allows the use of a mean diurnal profile. Future version of the algorithm will include diurnal variations from coincident SEVIRI observations for a more accurate representation of each fire's specificities.

Future developments will also include a parameterization of ground layer burning and peatland fires, to allow applications to boreal regions in particular.

The APIFLAME model may be applied to the analysis of past events or to the near-real time monitoring of emissions, providing area burned data are available. Daily emissions at 0.25° × 0.25° resolution for the 2003–2012 time period over Europe may be obtained from the CHARMEX project (Chemistry–Aerosol Mediterranean Experiment) page of the ECCAD database (http://eccad.pole-ether.fr).

Acknowledgements. This work was undertaken in the framework of the APIFLAME project, supported by the french research program PRIMEQUAL (project no. 0962C0068), and the APPAD projet funded by DGA. The French Ministry in charge of ecology is also acknowledged. The authors thank ECCAD and the CHARMEX project for including the inventory within the database. We also thank the MODIS land data teams and NASA LPDAAC for data availability, as well as Louis Giglio for his help using the MODIS fire data. Finally, the authors wish to thank Christine Wiedinmyer, Guido Van der Werf and Johannes Kaiser for the availability of their inventories and for helpful discussions.

The publication of this article is financed by CNRS-INSU.

References

Akagi, S. K., Yokelson, R. J., Wiedinmyer, C., Alvarado, M. J., Reid, J. S., Karl, T., Crounse, J. D., and Wennberg, P. O.: Emission factors for open and domestic biomass burning for use in atmospheric models, Atmos. Chem. Phys., 11, 4039–4072, doi:10.5194/acp-11-4039-2011, 2011. 5508, 5509, 5511, 5536

Alves, C., Gonçalves, C., Pio, C., Mirante, F., Caseiro, A., Tarelho, L., Freitas, M., and Viegas, D.: Smoke emissions from biomass burning in a Mediterranean shrubland, Atmos. Environ., 44, 3024–3033, doi:10.1016/j.atmosenv.2010.05.010, 2010. 5509

Alves, C., Vicente, A., Nunes, T., Gonçalves, C., Fernandes, A., Mirante, F., Tarelho, L., Sanchez de la Campa, A., Querol, X., Caseiro, A., Monteiro, C., Evtyugina, M., and Pio, C.: Summer 2009 wildfires in Portugal: emission of trace gases and aerosol composition, Atmos. Environ., 45, 641–649, doi:10.1016/j.atmosenv.2010.10.031, 2011. 5509

Amiridis, V., Giannakaki, E., Balis, D. S., Gerasopoulos, E., Pytharoulis, I., Zanis, P., Kazadzis, S., Melas, D., and Zerefos, C.: Smoke injection heights from agricultural burning in Eastern Europe as seen by CALIPSO, Atmos. Chem. Phys., 10, 11567–11576, doi:10.5194/acp-10-11567-2010, 2010. 5492

Anav, A., D'Andrea, F., Viovy, N., and Vuichard, N.: A validation of heat and carbon fluxes from high resolution land surface and regional models, J. Geophys. Res., 115, G04016, doi:10.1029/2009JG001178, 2010. 5497

Andreae, M. O. and Merlet, P.: Emission of trace gases and aerosols from biomass burning, Global Biogeochem. Cy., 15, 995–966, doi:10.1029/2000GB001382, 2001. 5492, 5508, 5511, 5536

Andreae, M. O., Rosenfeld, D., Artaxo, A., Costa, A. A., Frank, G. P., Longo, K. M., and Silva-Dias, M. A. F.: Smoking rain clouds over the Amazon, Science, 303, 1337–1342, doi:10.1126/science.1092779, 2004. 5492

Berrisford, P., Dee, D., Fielding, K., Fuentes, M., Kallberg, P., Kobayashi, S., and Uppala, S.: The ERA-Interim archive, ERA-40 Report Series No. 1, Tech. rep., ECMWF, Shinfield Park, Reading, 2009. 5497

EC: 2008 Directive 2008/50/EC of the European Parliament and of the council of 21 May 2008 on ambient air quality and cleaner air for Europe, European Parliament, Council, Official Journal L 152, 0001–0044, 2008. 5493

EEA: Technical report No17, CLC2006 technical guidelines, Tech. rep., European Environment Agency, Office for Official Publications of the European Communities, Copenhagen, 2007. 5495

Freeborn, P., Wooster, M., Hao, W., Ryan, C., Nordgren, B., Baker, S., and Ichoku, C.: Relationships between energy release, fuel mass loss, and trace gas and aerosol emissions during laboratory biomass fires, J. Geophys. Res., 113, D01301, doi:10.1029/2007JD008489, 2008. 5494, 5500

Friedl, M. A., Sulla-Menashe, D., Tan, B., Schneider, A., Ramankutty, N., Sibley, A., and Huang, X.: MODIS collection 5 global land cover: algorithm refinements and characterization of new datasets, Remote Sens. Environ., 114, 168–182, doi:10.1016/j.rse.2009.08.016, 2010. 5496

Gibbs, H.: Olson's major world ecosystem complexes ranked by carbon in live vegetation: an updated database using the GLC 2000 land cover product, available at: http://cdiac.ornl.gov/epubs/ndp/ndp017/ndp017b.html, last access: 31 October 2013, 2006. 5507

Giglio, L., Csiszar, I., and Justice, C. O.: Global distribution and seasonality of active fires as observed with the terra and aqua MODIS sensors, J. Geophys. Res., 111, G02016, doi:10.1029/2005JG000142, 2006. 5493, 5499

Giglio, L., Randerson, J. T., van der Werf, G. R., Kasibhatla, P. S., Collatz, G. J., Morton, D. C., and DeFries, R. S.: Assessing variability and long-term trends in burned area by merging multiple satellite fire products, Biogeosciences, 7, 1171–1186, doi:10.5194/bg-7-1171-2010, 2010. 5493, 5494, 5499, 5500, 5511, 5518

Grell, G., Freitas, S. R., Stuefer, M., and Fast, J.: Inclusion of biomass burning in WRF-Chem: impact of wildfires on weather forecasts, Atmos. Chem. Phys., 11, 5289–5303, doi:10.5194/acp-11-5289-2011, 2011. 5492

Hansen, M. C., DeFries, R. S., Townshend, J. R. G., Carroll, M., Dimiceli, C., and Sohlberg, R. A.: Global percent tree cover at a spatial resolution of 500 meters: first results of the MODIS vegetation continuous fields algorithm, Earth Interact., 7, 1–15, doi:10.1175/1087-3562(2003)007<0001:GPTCAA>2.0.CO;2, 2003. 5497, 5500

Hodnebrog, Ø., Solberg, S., Stordal, F., Svendby, T. M., Simpson, D., Gauss, M., Hilboll, A., Pfister, G. G., Turquety, S., Richter, A., Burrows, J. P., and Denier van der Gon, H. A. C.: Impact of forest fires, biogenic emissions and high temperatures on the elevated Eastern Mediterranean ozone levels during the hot summer of 2007, Atmos. Chem. Phys., 12, 8727–8750, doi:10.5194/acp-12-8727-2012, 2012. 5493, 5515

Hodzic, A., Madronich, S., Bohn, B., Massie, S., Menut, L., and Wiedinmyer, C.: Wildfire particulate matter in Europe during summer 2003: meso-scale modeling of smoke emissions, transport and radiative effects, Atmos. Chem. Phys., 7, 4043–4064, doi:10.5194/acp-7-4043-2007, 2007. 5493

Hoelzemann, J. J., Schultz, M. G., Brasseur, G. P., Granier, C., and Simon, M.: Global Wildland Fire Emission Model (GWEM): evaluating the use of global area burnt satellite data,

J. Geophys. Res., 109, D14S04, doi:10.1029/2003JD003666, 2004. 5493, 5498, 5507, 5508, 5510, 5533

Hyer, E. J. and Reid, J. S.: Baseline uncertainties in biomass burning emission models resulting from spatial error in satellite active fire location data, Geophys. Res. Lett., 36, L05802, doi:10.1029/2008GL036767, 2009. 5494, 5499

Jacob, D. and Podzun, R.: Sensitivity studies with the Regional Climate Model REMO, Meteorol. Atmos. Phys., 63, 119–129, 1997. 5497

Jaffe, D., Hafner, W., Chand, D., Westerling, A., and Spracklen, D.: Inter-annual variations in $PM_{2.5}$ due to wildfires in the Western United States, Environ. Sci. Technol., 42, 2812–2818, doi:10.1021/es702755v, 2008. 5492

Jaffe, D. A. and Wigder, N. L.: Ozone production from wildfires: a critical review, Atmos. Environ., 51, 1–10, doi:10.1016/j.atmosenv.2011.11.063, 2012. 5492

Kaiser, J. W., Heil, A., Andreae, M. O., Benedetti, A., Chubarova, N., Jones, L., Morcrette, J.-J., Razinger, M., Schultz, M. G., Suttie, M., and van der Werf, G. R.: Biomass burning emissions estimated with a global fire assimilation system based on observed fire radiative power, Biogeosciences, 9, 527–554, doi:10.5194/bg-9-527-2012, 2012. 5494, 5500, 5510

Konovalov, I. B., Beekmann, M., Kuznetsova, I. N., Yurova, A., and Zvyagintsev, A. M.: Atmospheric impacts of the 2010 Russian wildfires: integrating modelling and measurements of an extreme air pollution episode in the Moscow region, Atmos. Chem. Phys., 11, 10031–10056, doi:10.5194/acp-11-10031-2011, 2011. 5493

Koren, I., Kaufman, Y. R., Remer, L. A., and Martins, J. V.: Measurement of the effect of Amazon smoke on inhibition of cloud formation, Science, 303, 1342–1345, doi:10.1126/science.1089424, 2004. 5492

Krinner, G., Viovy, N., de Noblet-Ducoudré, N., Ogée, J., Polcher, J., Friedlingstein, P., Ciais, P., Sitch, S., and Prentice, I. C.: A dynamic global vegetation model for studies of the coupled atmosphere–biosphere system, Global Biogeochem. Cy., 19, GB1015, doi:10.1029/2003GB002199, 2005. 5495, 5497

Langmann, B., Duncan, B., Textor, C., Trentmann, J., and van der Werf, G.: Vegetation fire emissions and their impact on air pollution and climate, Atmos. Environ., 43, 107–116, doi:10.1016/j.atmosenv.2008.09.047, 2009. 5492, 5494

Li, F., Zeng, X. D., and Levis, S.: A process-based fire parameterization of intermediate complexity in a Dynamic Global Vegetation Model, Biogeosciences, 9, 2761–2780, doi:10.5194/bg-9-2761-2012, 2012. 5495, 5498

Maignan, F., Bréon, F.-M., Chevallier, F., Viovy, N., Ciais, P., Garrec, C., Trules, J., and Mancip, M.: Evaluation of a Global Vegetation Model using time series of satellite vegetation indices, Geosci. Model Dev., 4, 1103–1114, doi:10.5194/gmd-4-1103-2011, 2011. 5495, 5497

Mieville, A., Granier, C., Liousse, C., Guillaume, B., Mouillot, F., Lamarque, J.-F., Grégoire, J.-M., and Pétron, G.: Emissions of gases and particles from biomass burning during the 20th century using satellite data and an historical reconstruction, Atmos. Environ., 44, 1469–1477, doi:10.1016/j.atmosenv.2010.01.011, 2010. 5493

Mouillot, F. and Field, C.: Fire history and the global carbon budget: a 1 × 1 fire history reconstruction for the 20th century, Glob. Change Biol., 11, 398–420, doi:10.1111/j.1365-2486.2005.00920.x, 2006. 5499

Mu, M., Randerson, J. T., van der Werf, G. R., Giglio, L., Kasibhatla, P., Morton, D., Collatz, G. J., DeFries, R. S., Hyer, E. J., Prins, E. M., Griffith, D. W. T., Wunch, D., Toon, G. C., Sherlock, V., and Wennberg, P. O.: Daily and 3-hourly variability in global fire emissions and consequences for atmospheric model predictions of carbon monoxide, J. Geosphys. Res., 116, D24303, doi:10.1029/2011JD016245, 2011. 5505, 5510

Nachtergaele, F., van Velthuizen, H., Verekst, L., and Widberg, D.: Harmonized World Soil Database v 1.2., available at: http://webarchive.iiasa.ac.at/Research/LUC/External-World-soil-database/HTML/, last access: 31 October 2013, 2012. 5507

Panagos, P.: The European soil database, GEO:Connexion, 5, 32–33, 2006. 5498

Pereira, M., Trigo, R. M., da Camara, C. C., Pereira, J., and Leite, S. M.: Synoptic patterns associated with large summer forest fires in Portugal, Agr. Forest Meteorol., 129, 11–25, doi:10.1016/j.agrformet.2004.12.007, 2005. 5493

R'Honi, Y., Clarisse, L., Clerbaux, C., Hurtmans, D., Duflot, V., Turquety, S., Ngadi, Y., and Coheur, P.-F.: Exceptional emissions of NH_3 and HCOOH in the 2010 Russian wildfires, Atmos. Chem. Phys., 13, 4171–4181, doi:10.5194/acp-13-4171-2013, 2013. 5493

Roberts, G., Wooster, M. J., Perry, G. L. W., Drake, N., Rebelo, L.-M., and Dipotso, F.: Retrieval of biomass combustion rates and totals from fire radiative power observations: application to Southern Africa using geostationary SEVIRI imagery, J. Geophys. Res., 110, D21111, doi:10.1029/2005JD006018, 2005. 5500

Roberts, G., Wooster, M. J., and Lagoudakis, E.: Annual and diurnal african biomass burning temporal dynamics, Biogeosciences, 6, 849–866, doi:10.5194/bg-6-849-2009, 2009. 5505

Rosa, I. M. D., Pereira, J. M. C., and Tarantola, S.: Atmospheric emissions from vegetation fires in Portugal (1990–2008): estimates, uncertainty analysis, and sensitivity analysis, Atmos. Chem. Phys., 11, 2625–2640, doi:10.5194/acp-11-2625-2011, 2011. 5507

Roy, D. P., Boschetti, L., Justice, C. O., and Ju, J.: The collection 5 MODIS burned area product – global evaluation by comparison with the MODIS active fire product, Remote Sens. Environ., 112, 3690–3707, doi:10.1016/j.rse.2008.05.013, 2008. 5500

Roy, D. P., Boschetti, L., and Smith, A. M.: Satellite remote sensing of fires, in: Oxford Handbook of Innovation, edited by: Belcher, C. M., Oxford University Press, Oxford, 77–93, 2013. 5499

San-Miguel-Ayanz, J., Moreno, J. M., and Camia, A.: Analysis of large fires in European Mediterranean landscapes: lessons learned and perspectives, Forest Ecol. Manag., 294, 11–22, doi:10.1016/j.foreco.2012.10.050, 2013. 5493

Schmuck, G., San-Miguel-Ayanz, J., Camia, A., Durrant, T., Boca, R., and Libertà, G.: Forest fires in Europe, Middle East and North Africa 2012, Tech. rep., Joint Research Center, Institute for Environment and Sustainability, Via Enrico Fermi 2749, TP 261, 21027 Ispra (VA), Italy, doi:10.2788/58397, 2013. 5502

Seiler, W. and Crutzen, P. J.: Estimates of gross and net fluxes of carbon between the biosphere and the atmosphere from biomass burning, Climatic Change, 2, 207–247, doi:10.1007/BF00137988, 1980. 5492, 5494, 5495, 5505, 5520

Sitch, S., Smith, B., Prentice, I. C., Arneth, A., Bondeau, A., Cramer, W., Kaplan, J. O., Levis, S., Lucht, W., Sykes, M. T., Thonicke, K., and Venevsky, S.: Evaluation of ecosystem dynamics, plant geography and terrestrial carbon cycling in the LPJ dynamic global vegetation model, Glob. Change Biol., 9, 161–185, doi:10.1046/j.1365-2486.2003.00569.x, 2003. 5495

Sofiev, M., Vankevich, R., Lotjonen, M., Prank, M., Petukhov, V., Ermakova, T., Koskinen, J., and Kukkonen, J.: An operational system for the assimilation of the satellite information on wild-land fires for the needs of air quality modelling and forecasting, Atmos. Chem. Phys., 9, 6833–6847, doi:10.5194/acp-9-6833-2009, 2009. 5494, 5500

Soja, A. J., Cofer, W. R., Shugart, H. H., Sukhinin, A. I., Stackhouse, P. W. J., McRae, D. J., and Conard, S. G.: Estimating fire emissions and disparities in boreal Siberia (1998–2002), J. Geophys. Res., 109, D14S06, doi:10.1029/2004JD004570, 2004. 5498

Spracklen, D., Logan, J., Mickley, L., Park, R., Yevich, R., Westerling, A., and Jaffe, D.: Wildfires drive interannual variability of organic carbon aerosol in the Western US in summer, Geophys. Res. Lett., 34, L16816, doi:10.1029/2007GL030037, 2007. 5492

Stohl, A., Berg, T., Burkhart, J. F., Fjæraa, A. M., Forster, C., Herber, A., Hov, Ø., Lunder, C., McMillan, W. W., Oltmans, S., Shiobara, M., Simpson, D., Solberg, S., Stebel, K., Ström, J., Tørseth, K., Treffeisen, R., Virkkunen, K., and Yttri, K. E.: Arctic smoke – record high air pollution levels in the European Arctic due to agricultural fires in Eastern Europe in spring 2006, Atmos. Chem. Phys., 7, 511–534, doi:10.5194/acp-7-511-2007, 2007. 5492

Stroppiana, D., Brivio, P. A., Grégoire, J.-M., Liousse, C., Guillaume, B., Granier, C., Mieville, A., Chin, M., and Pétron, G.: Comparison of global inventories of CO emissions from biomass burning derived from remotely sensed data, Atmos. Chem. Phys., 10, 12173–12189, doi:10.5194/acp-10-12173-2010, 2010. 5494

Szopa, S., Hauglustaine, D. A., and Ciais, P.: Relative contributions of biomass burning emissions and atmospheric transport to carbon monoxide interannual variability, Geophys. Res. Lett., 34, L18810, doi:10.1029/2007GL030231, 2007. 5492

Tosca, M. G., Randerson, J. T., and Zender, C. S.: Global impact of smoke aerosols from landscape fires on climate and the Hadley circulation, Atmos. Chem. Phys., 13, 5227–5241, doi:10.5194/acp-13-5227-2013, 2013. 5492

Turquety, S.: The atmospheric impact of wildfires, in: Oxford Handbook of Innovation, edited by: Belcher, C. M., Oxford University Press, Oxford, 2013. 5492

Turquety, S., Logan, J., Jacob, D., Hudman, R., Leung, F., Heald, C., Yantosca, R., Wu, S., Emmons, L., Edwards, D., and Sachse, G.: Inventory of boreal fire emissions for North America in 2004: the importance of peat burning and pyro-convective injection, J. Geophys. Res., 112, D12S03, doi:10.1029/2006JD007281, 2007. 5499

Turquety, S., Hurtmans, D., Hadji-Lazaro, J., Coheur, P.-F., Clerbaux, C., Josset, D., and Tsamalis, C.: Tracking the emission and transport of pollution from wildfires using the IASI CO retrievals: analysis of the summer 2007 Greek fires, Atmos. Chem. Phys., 9, 4897–4913, doi:10.5194/acp-9-4897-2009, 2009. 5493, 5514

Urbanski, S. P., Hao, W. M., and Nordgren, B.: The wildland fire emission inventory: western United States emission estimates and an evaluation of uncertainty, Atmos. Chem. Phys., 11, 12973–13000, doi:10.5194/acp-11-12973-2011, 2011. 5494, 5518, 5522

van der Werf, G. R., Randerson, J. T., Giglio, L., Collatz, G. J., Kasibhatla, P. S., and Arellano Jr., A. F.: Interannual variability in global biomass burning emissions from 1997 to 2004, Atmos. Chem. Phys., 6, 3423–3441, doi:10.5194/acp-6-3423-2006, 2006. 5493, 5507 van der Werf, G. R., Randerson, J. T., Giglio, L., Collatz, G. J., Mu, M., Kasibhatla, P. S., Morton, D. C., DeFries, R. S., Jin, Y., and van Leeuwen, T. T.: Global fire emissions and the contribution of deforestation, savanna, forest, agricultural, and peat fires (1997–2009), Atmos. Chem. Phys., 10, 11707–11735, doi:10.5194/acp-10-11707-2010, 2010. 5493, 5494, 5506, 5510, 5518, 5522

Vestreng, V., Mareckova, K., Kakareka, S., Malchykhina, A., and Kukharchyk, T.: Inventory Review 2007; Emission Data reported to LRTAP Convention and NEC Directive, MSC-W Technical Report 1, Tech. rep., EMEP/MSC-W, Oslo, Norway, 2007. 5513

Wiedinmyer, C., Akagi, S. K., Yokelson, R. J., Emmons, L. K., Al-Saadi, J. A., Orlando, J. J., and Soja, A. J.: The Fire INventory from NCAR (FINN): a high resolution global model to estimate the emissions from open burning, Geosci. Model Dev., 4, 625–641, doi:10.5194/gmd-4-625-2011, 2011. 5494, 5500, 5510, 5519

Wooster, M., Roberts, G., Perry, G., and Kaufman, Y.: Retrieval of biomass combustion rates and totals from fire radiative power observations: calibration relationships between biomass consumption and fire radiative energy release, J. Geophys. Res., 110, D14311, doi:10.1029/2005JD006318, 2005. 5500

Yokelson, R. J., Griffith, D. W. T., and Ward, D. E.: Openpath Fourier transform infrared studies of large-scale laboratory biomass fires, J. Geophys. Res., 101, 21067–21080, doi:10.1029/96JD01800, 1996. 5507

Zobler, L.: A World Soil File for Global Climate Modelling. NASA Technical Memorandum 87802, Tech. rep., NASA Goddard Institute for Space Studies, New York, New York, USA, 1986. 5497

Table 1. Land cover categories in the CORINE land cover, and corresponding general ecozone and ORCHIDEE PFT. The applied weight is indicated in parentheses if different than 1.

Class	Vegetation type	Emission factor type	ORCHIDEE PFT
1	Arable land	Crop residue (25 %)	Agriculture (25 %)
2	Permanent crop	Crop residue	Agriculture
3	Pasture	Pasture (25 %), savanna (75 %)	Grass
4	Mixed cropland and other vegetation	Crop residue (50 %), savanna (50 %)	Agriculture (50 %), grass (50 %)
5	Mixed cropland and forest	Crop residue (50 %), forest (50 %)	Agriculture (50 %), forest
6	Forest: broad-leaved	Forest	Forest
7	Forest: coniferous	Forest	Forest
8	Forest: mixed	Forest	Forest
9	Natural grassland	Savanna	Grass
10	Moors and heathland	Savanna (70 %), forest (20 %), peat (10 %)	Forest, grass
11	Sclerophyllous vegetation	Chaparral	Forest, grass
12	Transitional woodland/shrubland	Savanna (50 %), forest (50 %)	Forest, grass
13	Peat bogs	Peatland	Forest, grass

Table 2. Comparison of total yearly burned area (km^2) by country from the EFFIS/JRC reports and this study (derived from MODIS MCD64).

Country	Database	2003	2004	2005	2006	2007	2008	2009	2010	2011	Correlation	Bias* (%)
Portugal	EFFIS	4257	1295	3383	755	314	172	874	1331	738	0.99	−24
	MCD64	4504	964	3330	863	138	57	550	1270	402		
Spain	EFFIS	1482	1342	1887	1488	820	503	1108	548	845	0.95	−32
	MCD64	1541	1212	1442	1294	365	189	697	232	541		
France	EFFIS	733	137	221	78	86	60	170	103	96	0.97	−20
	MCD64	584	83	163	36	30	119	118	141	23		
Italy	EFFIS	918	602	476	399	2277	663	733	465	720	0.79	−26
	MCD64	678	845	210	105	1293	813	391	464	331		
Greece	EFFIS	35	103	64	127	2257	292	353	90	291	0.99	75
	MCD64	65	220	96	272	3027	713	323	159	495		
Republic	EFFIS	NaN	N/A	N/A	N/A	327	59	13	7	173	0.92	−3
of Moldova	MCD64	5	14	17	12	334	65	0	10	62		
Bulgaria	EFFIS	50	11	15	35	430	53	23	65	69	0.66	887
	MCD64	228	442	149	638	768	351	52	193	239		
Romania	EFFIS	8	1	2	9	25	4	10	2	22	−0.1	20×10^3
	MCD64	157	462	313	752	688	2546	261	755	695		
Turkey	EFFIS	66	49	28	78	117	297	47	33	36	−0.35	5×10^3
	MCD64	967	1347	1271	1604	1393	1193	6787	3528	4732		

* $(A_M - A_E)/A_E \times 100$, with A_E and A_M are the total yearly burned area for one specific country reported by EFFIS and observed by MODIS, respectively.

Table 3. Fraction of vegetation available for burning in the considered carbon pools (following Hoelzemann et al., 2004). The minimum and maximum values are given in parentheses.

ORCHIDEE PFT	Litter	Leaf	Wood	Roots
Tropical broad-leaved evergreen	100	10 (5–20)	0	0
Tropical broad-leaved raingreen	100	10 (5–20)	0	0
Tropical needleleaf evergreen	100	30 (15–60)	10 (5–20)	0
Temperate broad-leaved evergreen	100	30 (15–60)	10 (5–20)	0
Temperate broad-leaved summergreen	100	20 (10–40)	10 (5–20)	0
Boreal needleleaf evergreen	70	20 (10–40)	20 (10–40)	5 (2.5–10)
Boreal broad-leaved summergreen	70	20 (10–40)	20 (10–40)	5 (2.5–10)
Boreal needleleaf summergreen	70	20 (10–40)	20 (10–40)	5 (2.5–10)
C3 grass	100	50 (25–100)	5 (2.5–10)	0
C4 grass	100	50 (25–100)	5 (2.5–10)	0
C3 agriculture	100	50 (25–100)	5 (2.5–10)	0
C4 agriculture	100	50 (25–100)	5 (2.5–10)	0

Table 4. Average summertime available fuel load in terms of carbon (kg m^{-2}) according to the regional ORCHIDEE simulation.

Scenario	Forest	Grassland	Agriculture
Min	4.69	0.98	2.94
Mean	6.69	1.17	2.97
Max	9.21	1.2	3.04
Var	6.93	1.17	2.99

Table 5. Average fuel load in terms of carbon (kg m^{-2}) according to the regional and global ORCHIDEE simulation with VAR scenario.

Simulation	Forest	Grassland	Agriculture
Regional	6.93	1.17	2.99
Global	3.66	1.48	2.67

Table 6. Emission factors (in $\mathrm{g\,kg^{-1}}$ DM) used for the species included in the inventory. All numbers are from the review by Akagi et al. (2011), except noted otherwise.

Species	Tropical Forest	Savanna	Crop residue	Pasture Maintenance	Boreal forest	Temperate forest	Peatland	Chaparral
CO_2	1643	1686	1585	1548	1489	1637	1563	1710
CO	93	63	102	135	127	89	182	67
CH_4	5.07	1.94	5.82	8.71	5.96	3.92	11.8	2.51
C_2H_2	0.44	0.24	0.27	0.21	0.18	0.29	0.14	0.20
C_2H_4	1.06	0.82	1.46	1.28	1.42	1.12	1.79	0.75
C_2H_6	0.71	0.66	0.91	0.95	1.79	1.12	–	0.36
C_3H_4	0.02	0.01	–	0.02	–	–	–	–
C_3H_6	0.64	0.79	0.68	0.85	1.13	0.95	2.30	0.38
C_3H_4	–	–	–	–	0.06[g]	–	–	–
C_3H_8	0.13	0.10	0.28	0.22	0.44	0.26	–	0.19
Isoprene	0.13	0.04	0.38	0.12	0.15[g]	–	1.07	–
C_6H_6	0.39	0.20	0.15	0.70	1.11[g]	–	2.46	–
Toluene	0.26	0.08	0.19	0.34	0.48[g]	–	1.21	–
Xylene	0.11	0.01	–	0.11	0.18[g]	–	-	–
Terpenes	–	–	–	–	3.09[g]	–	–	–
C_2H_5OH	–	–	–	–	0.05[g]	–	–	–
CH_3OH	2.43	1.18	3.29	5.84	2.82	1.93	5.36	0.80
Phenol	0.45	0.52	0.52	1.68	2.96	0.33	4.36	0.45
HCHO	1.73	0.73	2.08	1.90	1.86	2.27	1.69	0.83
CH_3COCH_3	0.63	0.16	0.45	1.05	0.75[g]	–	1.08	–
MVE	–	0.16	0.08	–	–	–	0.85	–
Acetic acid	4.08	3.82	6.89	10.66	5.15	2.43	7.78	1.178
OCS	0.02	–	–	–	0.46[g]	–	1.20	–
NH_3	1.33	0.52	2.17	1.47	2.72	0.78	10.8	1.03
123TMB	–	–	–	–	0.05[g]	–	–	–
124TMB	–	–	–	–	0.03[g]	–	–	–
135TMB	–	–	–	–	5.86E-03[g]	–	–	–
AROM[a]	0.06	0.01	–	–	0.13[g]	–	–	–
ALKA[b]	0.07	0.04	0.15	0.06	0.35	0.08	–	0.14
ALKEN[c]	0.30	0.16	0.50	0.37	0.48	–	–	–
ALDEHS[d]	2.26	1.16	2.71	2.78	0.62	0.18	4.73	0.17
KETON[e]	1.06	–	–	3.5	0.43[g]	–	–	–
FURANS[f]	2.29	0.17	0.11	2.63	0.8	0.2	1.51	0.18
SO_2	0.40	0.48	0.4[h]	0.32	1.[g,h]	1.[g,h]	–	0.68
HONO	1.18	0.20	0.	0.16	0.	0.52	0.	0.41
NO_X	2.55	3.9	3.11	0.75	0.90	2.51	0.8	3.26
N_2O	–	–	–	–	0.41	0.16	–	0.25
BC	0.52	0.37	0.75	0.91	–	0.56[g]	0.20	1.3
OC	4.71	2.62	2.30	9.64	–	9.2[g]	6.23	3.7
$PM_{2.5}$	9.1	7.17	6.26	14.8	15.3	12.7	-	11.9
Total PM	18.5	8.5[h]	6.26[h]	28.9	17.6[g,h]	17.6[g,h]	–	–

[a] AROM: the aromatics other than benzene, toluene, and trimethylbenzene (Molar mass $M = 126\,\mathrm{g\,mol^{-1}}$);
[b] ALKAN: butanes and heavier alcanes ($M = 58\,\mathrm{g\,mol^{-1}}$);
[c] ALKEN: butenes and heavier alcenes ($M = 56\,\mathrm{g\,mol^{-1}}$);
[d] ALDEHS: aldehydes other than formaldehyde ($M = 44\,\mathrm{g\,mol^{-1}}$);
[e] KETONS: cetones other than acetone ($M = 72\,\mathrm{g\,mol^{-1}}$);
[f] FURANS: furans ($M = 82\,\mathrm{g\,mol^{-1}}$);
[g] Values for extratropical forest, also used for temperate forests;
[h] Values from Andreae and Merlet (2001).

Table 7. Approaches and parameters used in the inventories compared. AB stands for area burned, NB for the number of active fires, and FRP for the fire radiative power.

	APIFLAMEv1	GFEDv3	FINNv1	GFASv1
Method	Eq. (1) Daily 500 m	Eq. (1) Daily, 3 h $0.5^\circ \times 0.5^\circ$	Eq. (1) Daily 1 km	Top-down Daily $0.5^\circ \times 0.5^\circ$
Fire data	AB MCD64	AB, NB MCD64, MOD14	NB MOD14	FRP MOD14
F_v	ORCHIDEE model	CASA-GFED model	Tabulated	Function of FRP
$E_{v,i}$ (main source)	Akagi et al. (2011)	Andreae and Merlet (2001)	Akagi et al. (2011)	Andreae and Merlet (2001)

Table 8. Partitioning of area burned (AB) and CO emissions for each CLC category, on average over the 2003–2010 time period, and in the Euro-Mediterranean area. The sum over large vegetation types is provided in the last lines of the table. About 1 % of emissions are in other classes.

Class	AB (%)	CO (%)	NO_X (%)
1	33.6	16.1	14.6
2	19.3	23.3	20.0
3	0.9	0.7	0.8
4	3.7	5.7	6.2
5	0.7	1	0.9
6	4.7	9.0	7.5
7	3.0	4.8	3.9
8	2.6	4.1	3.4
9	9.5	6.4	9.0
10	1.5	3.0	3.4
11	5.2	5.4	6.5
12	13.2	19.6	22.8
Cropland	55	43	38
Pasture	1	1	1
Forest	11	18	15
Savanna	12	9	12
Shrubland	20	28	33

Table 9. Average (2003–2012) total annual emissions in Gg for different pollutants and regions of the Euro-Mediterranean. The average total emissions from the GFED and GFAS inventories are provided for comparison (correlation of the daily and monthly emissions are provided in parenthesis).

Species	Western Eu.	Central Eu.	Eastern Eu.	Euro-Med.	GFED[a]	GFAS
CO	1013	404	1164	2581	696	1376
NO_X	40	15	39	94	24	43
NMVOCs	182	76	231	489	68[b]	455
NH_3	15	6	21	42	66	19
SO_2	8	3	7	18	6	8
OC	58	20	40	118	48	76
BC	11	4	9	24	5	9
TPM	156	55	115	326	121	195

[a] Average for years 2003–2010 for the GFED inventory;

[b] NMHC in the GFED inventory.

Table 10. Average (2003–2011) total annual emissions in Gg by country for the main pollutants, for the fire emissions (F) and the EMEP anthropogenic emissions (A). Only countries for which fire CO emissions are larger than 30 Gg yr^{-1} on average, and for which anthropogenic emissions are available in the EMEP inventory, are reported.

Country	CO		NO_X		NMVOCs		NH_3		SO_2		$PM_{2.5}$		PM coarse*	
	F	A	F	A	F	A	F	A	F	A	F	A	F	A
Albania	100	128	3	26	17	30	2	25	1	35	13	13	2	4
Bulgaria	65	315	2	139	13	88	1	56	0.4	654	6	30	1	21
Bosnia-Herzegovina	75	116	3	52	13	42	1	17	0.7	429	10	19	2	25
Spain	294	1997	12	1133	53	752	4	373	3	902	39	85	8	38
France	40	4634	2	1269	7	1059	1	661	0.3	382	5	274	1	117
Greece	186	666	7	382	35	219	3	66	1	456	21	57	3	33
Croatia	17	326	1	78	3	94	0.2	39	0.1	57	2	11	0.5	5
Italy	156	3160	6	1113	30	1223	2	408	1	338	15	167	2	30
Republic of Moldova	38	126	1	30	8	35	1	26	0.1	12	2	6	0.01	3
Macedonia	41	95	1	36	7	28	1	9	0.3	105	5	9	1	9
Portugal	700	513	28	224	125	198	11	49	6	126	91	58	17	25
Romania	66	1264	2	300	13	441	1	185	0.3	584	5	110	0.4	28
Ukraine	1727	2817	53	592	357	338	36	179	7	1279	107	228	1	162
Turkey	573	3549	20	1122	115	1080	10	431	3	1551	44	256	5	99
Total	4077	19 708	141	6497	799	5627	74	2524	23	6910	367	1322	44	600

* TPM–$PM_{2.5}$ in fire inventory.

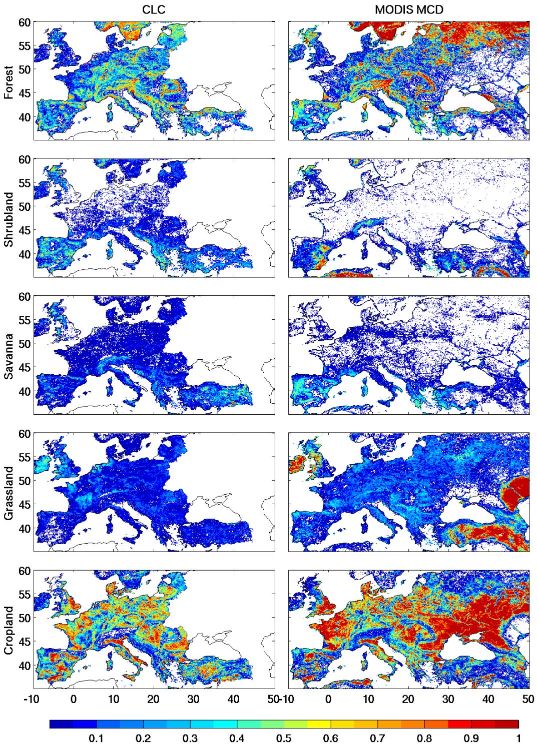

Fig. 1. Fraction of vegetation cover for grouped vegetation types and the CLC and MODIS MCD12 databases (reference year 2006), averaged on a 0.1° × 0.1° grid. For CLC, savanna corresponds to natural grassland and grassland to pasture, for MODIS MCD12, specific vegetation types are assigned to shrubland, savanna and grassland. White areas to the east of the domain in the CLC maps correspond to unavailable data.

Title Page
Abstract
Introduction
Conclusions
References
Tables
Figures
◀◀
▶▶
◀
▶
Back
Close
Full Screen / Esc
Printer-friendly Version
Interactive Discussion

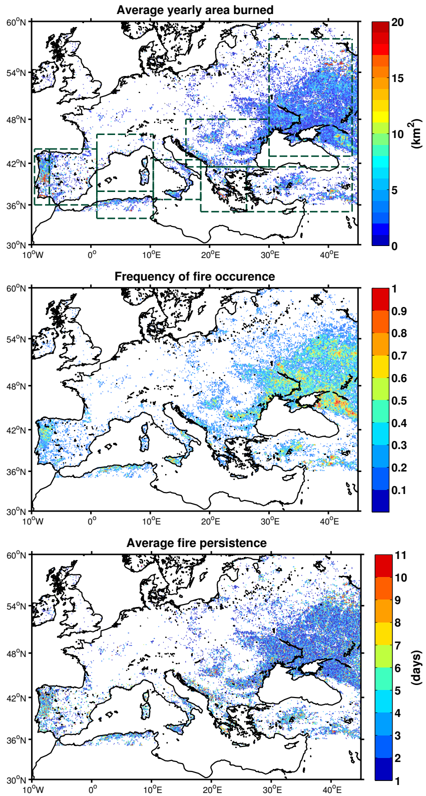

Fig. 2. Averaged total yearly burned area on a 0.1° × 0.1° grid according to the MODIS MCD64 product for the 2003–2012 time period, corresponding frequency of fire occurrence, and average duration of the fire events within each grid cell. Regions used for the statistical analysis are indicated on the top panel.

Title Page
Abstract
Introduction
Conclusions
References
Tables
Figures
◀▮ ▶▮
◀ ▶
Back
Close
Full Screen / Esc
Printer-friendly Version
Interactive Discussion

Title Page
Abstract
Introduction
Conclusions
References
Tables
Figures
◀◀
▶▶
◀
▶
Back
Close
Full Screen / Esc
Printer-friendly Version
Interactive Discussion

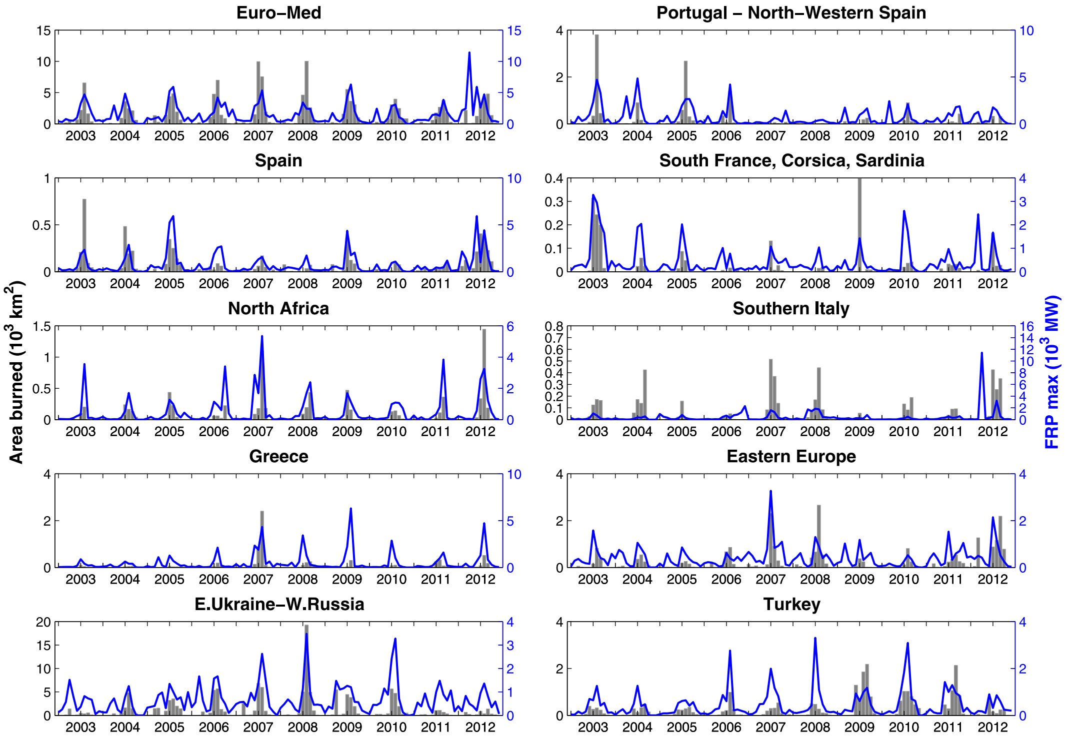

Fig. 3. Monthly burned area (bar plot) according to the MODIS MCD64 product for the 2003–2012 time period and within the main burning subregions. The corresponding maximum FRP detected is also plotted (solid line). Ticks on the *x* axis correspond to January and July.

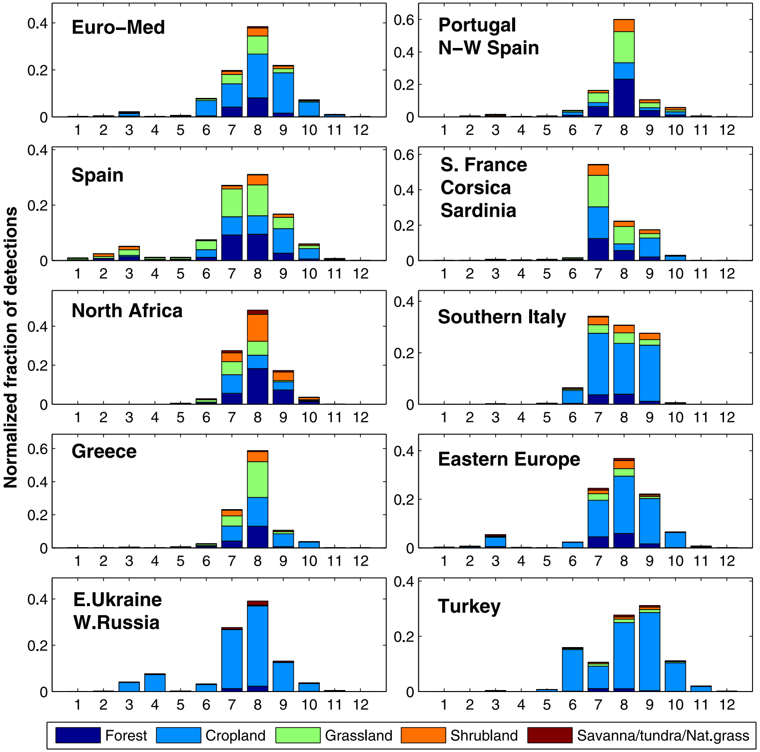

Fig. 4. Fraction of area burned detections located in different vegetation types for the CLC (grouped vegetation classes). For North Africa, Ukraine and Russia, the MODIS land cover is used.

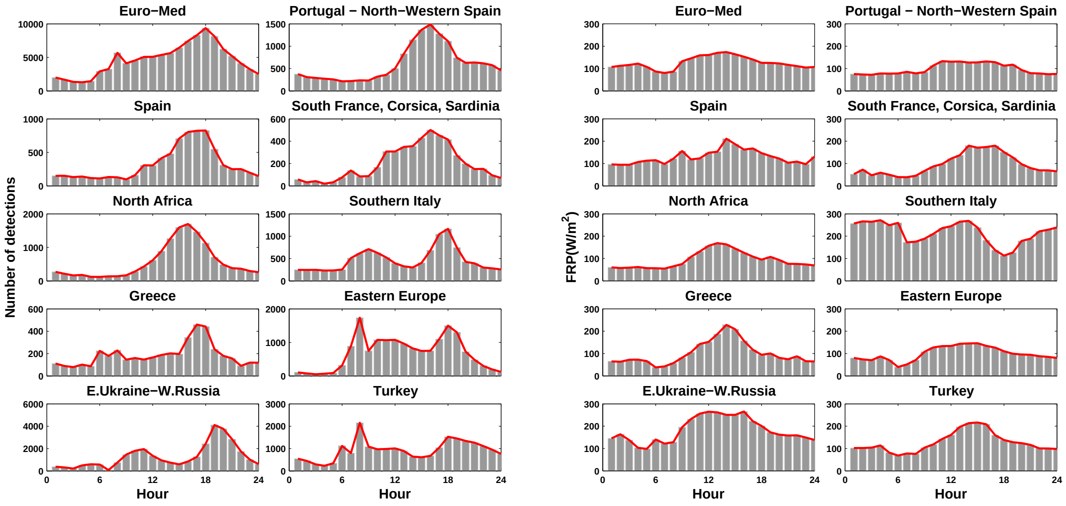

Fig. 5. Hourly variation of the number of fires detected by the MSG/SEVIRI instrument (left pannel) and of the average FRP measurements over several subregions of the domain for the 2008–2010 time period (July–August only). The red line shows the corresponding averaged diurnal cycle.

Title Page
Abstract
Introduction
Conclusions
References
Tables
Figures
◀
▶
Back
Close
Full Screen / Esc
Printer-friendly Version
Interactive Discussion

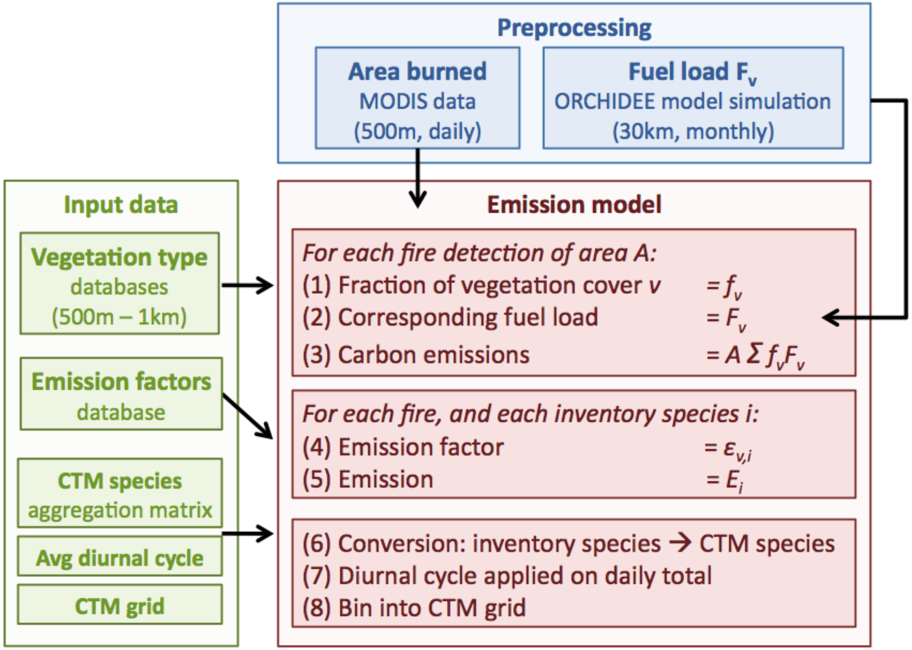

Fig. 6. Schematic representation of the APIFLAME emissions' model.

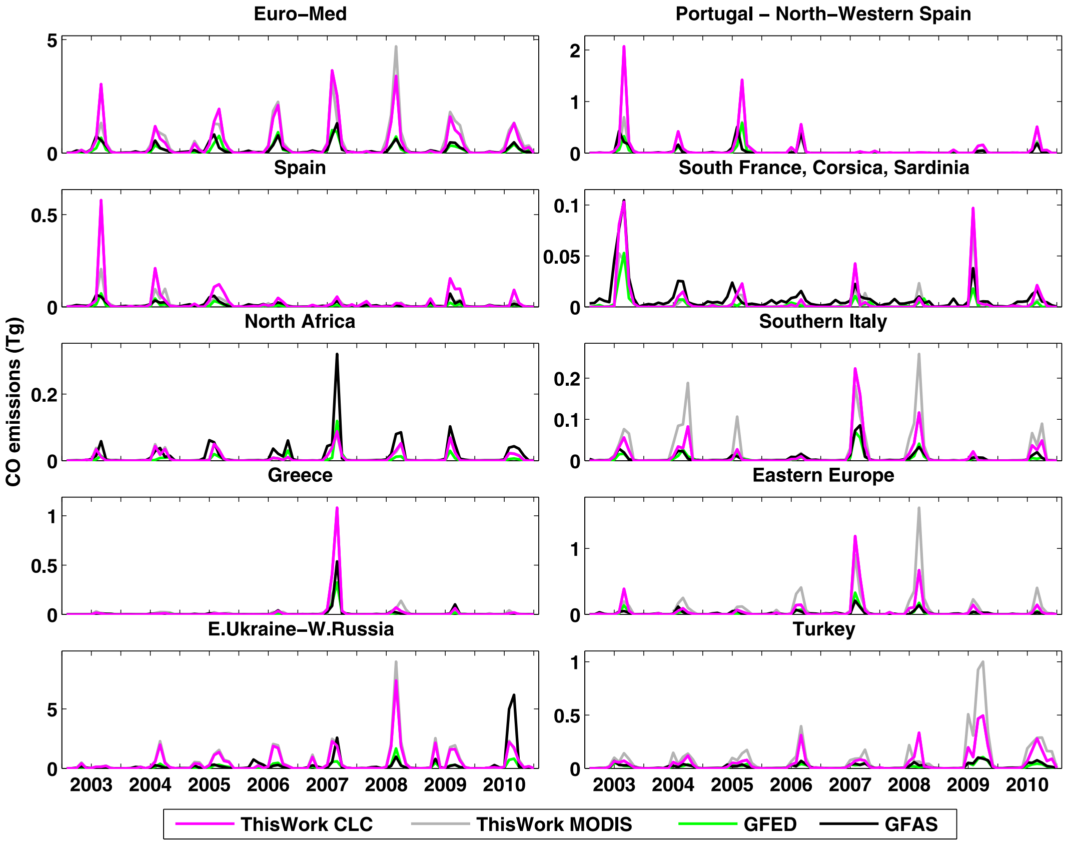

Fig. 7. Monthly emissions of CO in several subregions of Europe and the Mediterranean area according to this work, using CLC or MODIS MCD12 vegetation databases, and according to the GFEDv3 and the GFASv1 inventories.

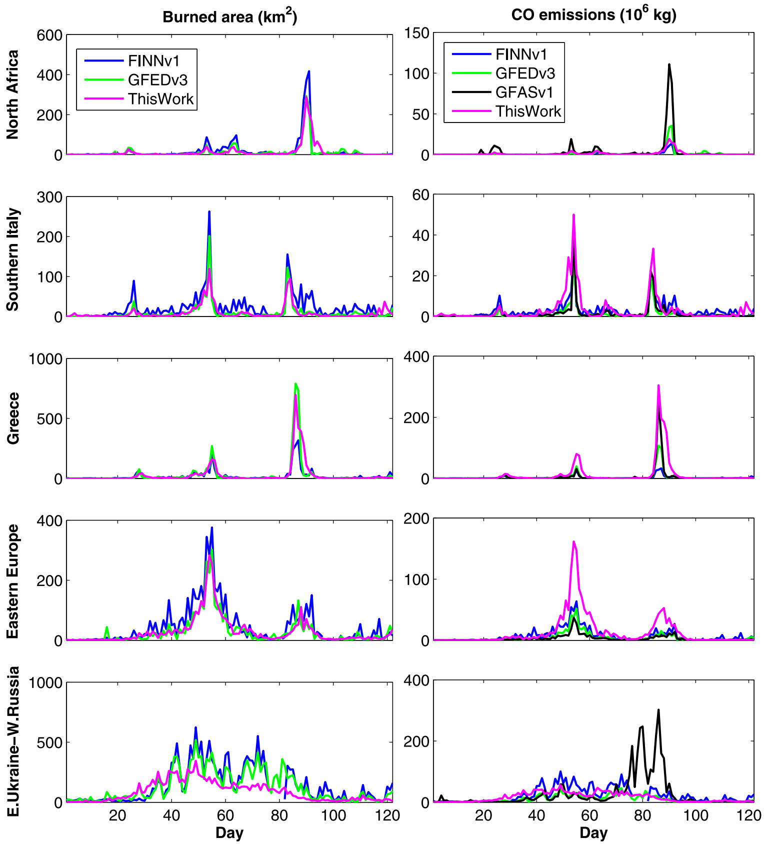

Fig. 8. Daily burned area (left) and carbon monoxide (CO) emissions (right) during the summer 2007 within subregions of Fig. 2 according to the present work and the FINN-v1 and GFED-v3 inventories.

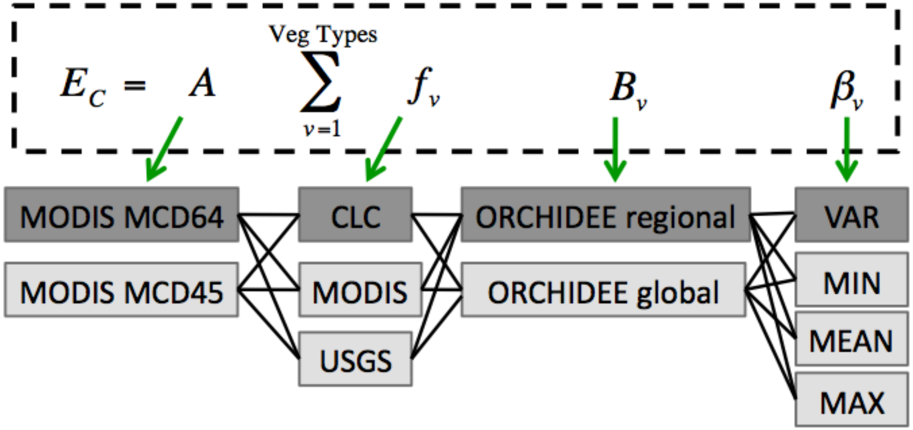

Fig. 9. Schematic representation of the 48 configurations used for the ensemble calculation of carbon emissions. The 4 scenarios for the fraction of biomass available for burning β are: minimum efficiency (MIN), maximum (MAX), average (MEAN) and varying depending on moisture stress (VAR). The dark gray boxes correspond to the default options for each of the parameters.

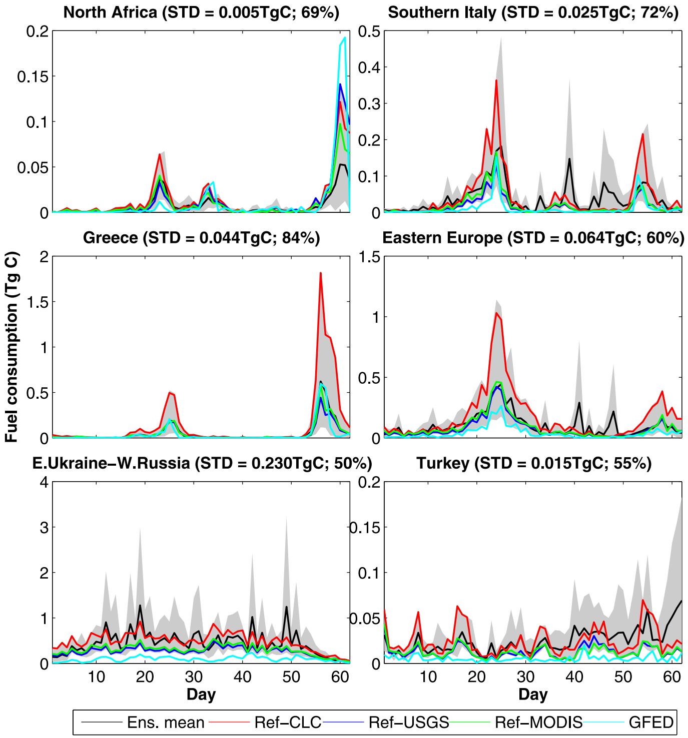

Fig. 10. Daily fuel consumption for the ensemble mean, and the reference configuration and either CLC, MODIS or USGS landcover types for July–August 2007. The spread of the ensemble is indicated by the shaded gray area. The values from the GFED inventory are also plotted for comparison. The average standard deviation (absolute value and relative to the ensemble mean) is indicated on top of each plot.

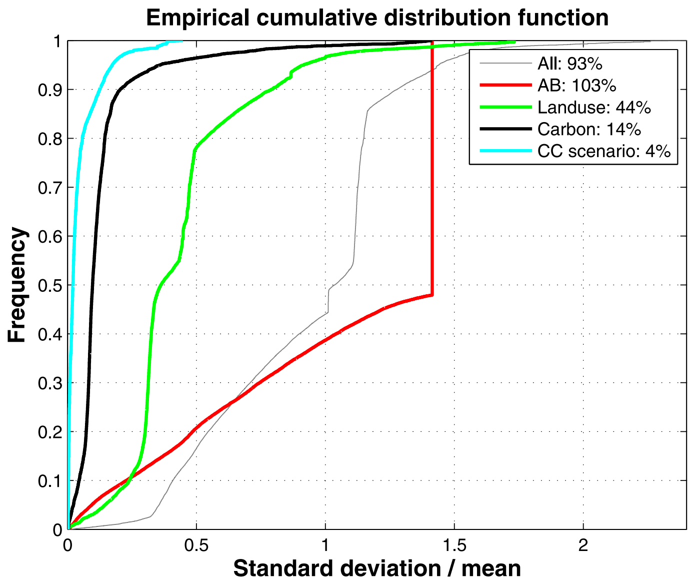

Fig. 11. Cumulative density functions (CDF) of the standard deviation of the ensemble results for daily emissions (relative to the ensemble average). CDF for the 48 estimates is indicated in gray. The CDFs for calculations with the reference configuration and one varying parameter are also indicated, with the following parameters considered individually: area burned (AB), vegetation database (landuse), biomass density (Carbon), scenario of combustion completeness (CC scenario).